12-3-2015

Characterization of Viral RNA-Induced Protein Kinase R Dimerization and Activation

Bushra Husain
University of Connecticut - Storrs, bushrahusain@gmail.com

Characterization Of Viral RNA-Induced Protein Kinase R Dimerization And Activation

Bushra Husain, PhD

University of Connecticut, 2015

Protein kinase R (PKR) is a key component of the interferon-induced immune response to viral stress. It contains two N-terminal dsRNA binding domains (dsRBD) and a C-terminal serine/threonine kinase domain separated by a 90 residue unstructured linker of unknown function. PKR is activated by viral dsRNAs via dimerization and autophosphorylation of specific serine and threonine residues. We have developed an assay to measure dimerization of PKR while bound to various dsRNAs using Förster resonance energy transfer. This is the first direct measurement of PKR dimerization upon dsRNAs binding. Our results show that inactive dimers of PKR exist in solution, and that a specific back-to-back dimer configuration is essential for activation. The role of the interdomain linker was determined by characterizing linker-deleted constructs of PKR. We propose that the unstructured linker may exist to negatively regulate PKR activation by limiting it's binding stoichiometry and curbing dsRNA-independent activation. The role of the second dsRNA binding domain was probed by mutating residues likely to contact dsRNA. Collectively, the studies presented here provide new insight on the elusive mechanism of dsRNA induced PKR activation.

Characterization Of Viral RNA-Induced Protein Kinase R Dimerization And Activation

Bushra Husain

B.Tech, Anna University, 2008

A Dissertation

Submitted in Partial Fulfillment of the

Doctor of Philosophy at the

University of Connecticut

2015

APPROVAL PAGE

Characterization Of Viral RNA-Induced Protein Kinase R Dimerization And Activation

Presented by

Bushra Husain, B.Tech.

Major Advisor_____

James L. Cole

Associate Advisor_____

Nathan N. Alder

Associate Advisor_____

Carolyn M. Teschke

University of Connecticut

2015

Acknowledgements

I would like to sincerely thank my advisor Dr. James L. Cole for his wholehearted support and encouragement over the last six years. I am truly grateful to him for giving me the opportunity to work on diverse and fascinating projects, with the chance to learn a variety of biophysical techniques. My progress and successes are due in large part to his strong mentorship and guidance.

I want to thank the rest of my committee: Dr. Carolyn Teschke, Dr. Nathan Alder, Dr. Victoria Robinson and Dr. Ishita Mukerji for their helpful ideas and suggestions. I sincerely appreciate their willingness to meet and council me despite their demanding schedules. They have served as outstanding role models and have pushed me to think critically and clearly. I thank my lab mates, past and present: Andy, Cassie, Chris, David, Eric, Jason, Katie and Steve for making my days in the lab so enjoyable, even when experiments did not always go as planned. Your kindness and consideration have shown me what it means to be a part of a team.

I also thank Mike and Matthew, two talented undergraduate students whom I had the opportunity to mentor. Thank you to Jeff Lary for patiently teaching me the nuts and bolts of AUC data collection and analysis. I would like to thank Megan DeLivron, who introduced me to molecular biology, and whose warmth and kindness will never be forgotten. I thank Mark W. Maciejewski and Vitaliy Gorbatyuk for helping me conduct my first NMR experiments and for answering numerous questions on data analysis. I thank Anne St Onge for being a constant source of positivity and for looking out for me on more occasions than one. Thank you to Linda, Maryke and Jane for their hard work and

assistance. I would like to express my sincere gratitude to Xinnian Chen and Penny Dobbins for giving me my first teaching position at the University of Connecticut.

I would like to thank my friends within and outside MCB: Ananya, Apurba Robbins, Tenil, Nidhish and many others for making UCONN my home away from home.

Lastly, I would like to thank my family for their unconditional love and unswerving belief in my abilities. They are truly my strength and my comfort. I cannot imagine being here today without them. I am truly thankful to my sister Athiya for her constant words of encouragement and her generosity. I especially thank my mother, Abida, who has been the source of my joy and inspiration and to whom this thesis is dedicated.

Table of Contents

List of Figures

Chapter 6:

List of Tables

Chapter 1: Introduction

1.1 Role of PKR in immune response and signaling

Protein kinase R is a critical component of the innate immune response to a variety of stress stimuli such as viral infection[1]. It exists endogenously in host cells in a latent inactive state and is over-expressed upon induction by type I interferon[2]. PKR contains tandem N-terminal dsRNA binding domains separated by a 20-residue linker and a C-terminal kinase domain. The kinase and dsRNA binding domains are separated by a long unstructured linker of ~90 residues in length. PKR recognizes and binds to viral RNAs that are generated in the cell as a by-product of viral replication[3,4], and becomes activated via dimerization and autophosphorylation[5]. Activated PKR phosphorylates eIF2α, which impairs the initiation of translation of host and viral proteins in the cell[6]. eIF2A is a heterotrimeric complex comprising of α, β and γ subunits. In the GTP bound form and in the presence of eIF2B it is able to bind to the initiating Met-tRNA and can transfer the tRNA to the 40S ribosome to initiate protein translation via GTP-GDP exchange[7]. Phosphorylation of eIF2α at S51 locks the subunit in a GDP-bound state incapable of binding to the Met-tRNA and initiating protein translation. Consequently the translational machinery is unable to synthesize viral and host proteins eventually leading to apoptosis, thus containing the spread of the infection. In addition to the eIF2α phosphorylation, PKR participates in a myriad of cellular signaling pathways, which relate to cell proliferation, tumor suppression, and activation of transcription factors such as interferon[8]. In the absence of stimulus the transcription factor NFκB is sequestered in the cytosol by two inhibitory proteins IκBα and IκBβ in the cytosol[9]. The binding of these

proteins block the nuclear localization sequence as well as the DNA binding region of NFκB thus inhibiting its ability to serve as a transcriptional regulator. Phosphorylation the of the IκB proteins at specific serine and threonine positions lead to the dissociation from NFκB and they are then tagged for proteasomal degradation via polyubiquitnation. IκB phosphorylation is mediated by IKK (IκB kinases), which is a substrate of active PKR. Phosphorylated PKR activates IKK and mediates the release of NFκB, which can transcriptionally regulate various genes involved in immunity, inflammation, cell proliferation and differentiation among many[10].

1.2. Mechanism of PKR activation by dsRNA

PKR binds to dsRNA in a sequence non-specific manner and binds most strongly to perfect duplexes[3]. The dsRNA binding domains of PKR are members of a large family of homologous domains, including Xlrbpa2 from *Xenopus laevis*. The crystal structure of Xlrbpa2 in complex with 16 bp duplex show that the intermolecular interactions are primarily between positively charged residues on the dsRBD and backbone phosphodiester oxygen and 2'-OH groups on the dsRNA. Xlrbpa2, which is a single dsRBD, makes contacts within two minor grooves and the adjoining major groove and has a footprint of 16 bp[11]. PKR contains two such dsRBDs. PKR is activated by dsRNAs in a length dependent manner. The shortest dsRNA that can activate PKR is 30 bp[12,13]. Activation follows a "bell-shaped" pattern as a function of dsRNA concentration due to the inhibition of PKR activation at high dsRNA concentrations[14,15].

Mechanism of PKR activation by variable length duplex RNAs

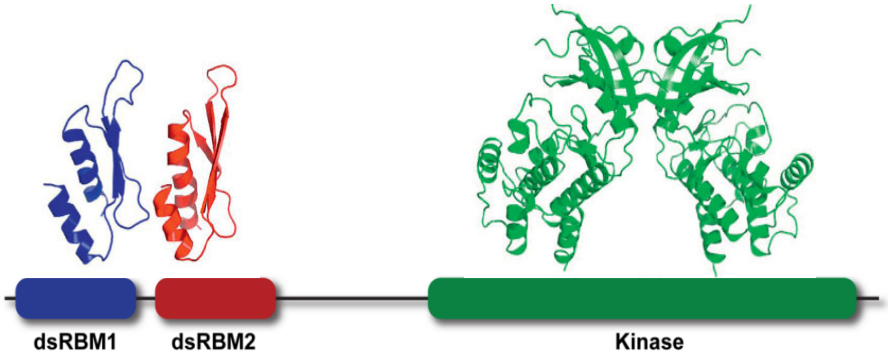

Fig. 1.1. Domain organization of PKR.

PKR is a member of the host anti-viral interferon induced defense pathway and is activated upon binding to viral dsRNA containing complex secondary structural features[16]. PKR consists of a C-terminal kinase domain and an N-terminal dsRBD separated by a 90 residue unstructured linker (Figure 1.1.). The N terminal lobe of the kinase is involved in forming the dimer interface and the C terminal lobe contains the substrate recognition site for eIF2α[17]. The nucleotide-binding site is located in between the two lobes. The dsRBD consists of tandem dsRNA binding motifs (dsRBM) 1 and 2, each having the conserved αββββα fold separated by a short linker[18]. The structures of the kinase domain[17] and dsRBD[18] have been solved by X-ray crystallography and NMR, respectively. No structure of full length PKR is available.

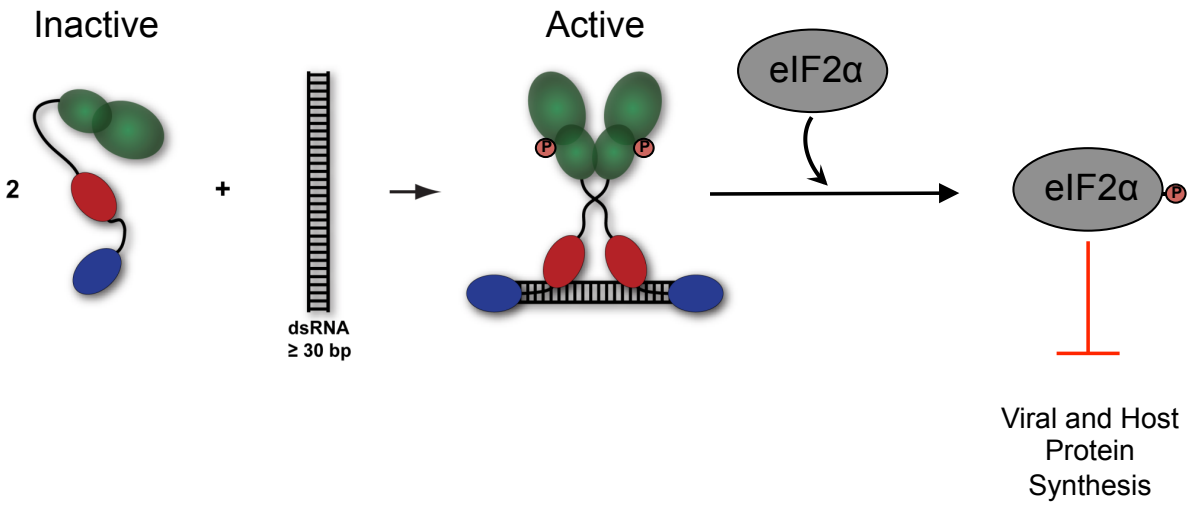

Fig. 1.2. Dimerization model for PKR activation by dsRNAs ≥ 30 bp.

PKR is biased to binding A-form dsRNA[19]. Studies performed previously have revealed that the 30 bp duplex is the minimum length dsRNA that can activate PKR (Figure 2). It is also the minimum length required for the binding of two PKR monomers[13]. These results led to the proposal of the dimerization model for PKR activation by duplex RNAs in which the role of the dsRNA is to bind two PKR monomers, leading to dimerization and activation.

The effect of salt concentration on the stoichiometry and binding affinity of PKR to dsRNA has been studied previously[13]. It was observed that a decrease in the NaCl concentration from 200 mM to 75 mM leads to a considerable increase in binding affinity as determined by sedimentation velocity and fluorescence anisotropy experiments.

Constructs of the dsRBM1 alone and the dsRBD have been studied for their interaction with variable length duplex RNAs[20]. The stoichiometry with which the dsRBM1 binds dsRNA increases sequentially with RNA length as a result of the

increase in number of available configurations. However, the dsRBD consisting of both motifs does not display the same trend. The stoichiometry of binding increases systematically from 15-35 bp, and then decreases with dsRNAs longer than 35 bp. This indicates a greater site size on longer activating duplexes relative to shorter non-activating sequences. ^{1}H-^{15}N HSQC NMR spectra of the dsRBD have been examined upon titration with 20 bp and 40 bp dsRNAs. The resonances most affected upon 20 bp interactions correspond to regions in the dsRBM1 and the N-terminus of the dsRBM2. However upon 40 bp titration residues corresponding to both the dsRNA binding motifs showed significant chemical shifts, indicating that the dsRBM2 makes additional interactions with longer, activating dsRNAs.

1.3. RNAs that interact with PKR *in vivo*

Several viral and cellular RNAs have been found to activate PKR. The internal ribosome entry site (IRES) RNA produced by the Hepatitis C virus consists of several domains with complex secondary structural elements such as internal loops, bulges and a pseudoknot[21,22]. At least one of the domains has been found to activate PKR through a partial structural mimicry of A-form dsRNA. The 3'-UTR of tumor necrosis factor – α (TNF- α) mRNA has also been found to activate PKR indicating that cellular regulation of PKR also occurs[23]. Several viruses have developed mechanisms to block the activation of PKR and its downstream signaling processes. Adenovirus and Epstein Barr virus (EBV) produce inhibitory RNAs that abrogate PKR dimerization and activation[24,25]. Adenovirus VAI consists of three domains: an apical stem, a central domain and a terminal stem. VAI as well as the mutant of VAI lacking the terminal stem inhibit PKR

activation to the same extent. Interestingly it was shown that the apical stem and central domains of PKR together form a site for the binding of a single PKR molecule[26,27].

One of the most well studied dsRNAs that interact with PKR is the human immunodeficiency virus type - 1 transactivation-responsive region (TAR) RNA[28-30]. It is a 23 bp stem loop RNA with three bulges that is known to dimerize. The TAR dimer consists of a 46 bp duplex region with an internal loop. Monomeric TAR is an inhibitor of PKR, whereas the TAR dimer is known to activate PKR (Figure 3). Sedimentation velocity studies reveal that the TAR dimer is capable of binding two monomers of PKR thereby allowing PKR dimerization and activation. This is also indicative of PKR's ability to accommodate internal loops or barriers to dimerization.

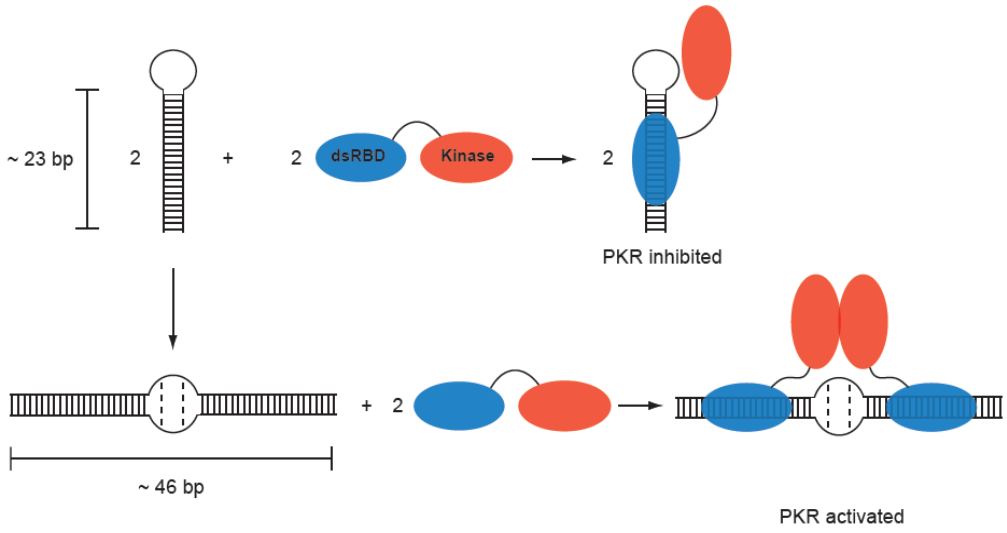

Fig. 1.3.Mechanism of activation of PKR by TAR RNA dimer.

1.4.Correlation between dimerization and autophosphorylation

The mechanism for dsRNA-induced PKR activation involves the formation a specific back-to-back dimer interface that was observed in the crystal structures of the kinase

domains bound to eIF2α[17]. PKR dimerizes weakly in the solution and can be activated in the absence of dsRNA[31]. Activation results in the autophosphorylation of specific serine and threonine residues within the kinase[32,33]. T446 in the activation segment is critical for the active enzyme and K296 is essential for phosphotransfer near the ATP binding site. The kinase domain of PKR (258-551) has a canonical bilobal architecture. The N-lobe comprises of a five-stranded antiparallel β sheet and two helices α0 and αC. The residues that form the dimer interface reside exclusively within the N-lobe, many of which are in the helix αC. The C-lobe is larger containing eight α helices and two β strands. The N-terminal region of the helix αG in the C-lobe as well as residues within the activation segment make specific contacts with PKR's substrate eIF2α. The ATP binding site exists in the cleft between the two lobes. K296-E308 ion pair in the active site aid in coordinating the nucleotide moiety and for phosphotranfer. K296R mutants are catalytically inactive but are still able to bind nucleotides. Threonine 446 within the activation segment of the kinase domain dimers are phosphorylated in the structure. K304 and R307 side chains protruding from the helix αC and R416 from the C lobe coordinate phosphorylated T446. Therefore, the specific configuration of helix αC may be critical for facilitating the formation of the active enzyme. Mutational analysis of residues within the dimer interface perturbed and in some cases abolished PKR activation. The dimer interface is held together by a number of residues specifically a salt bridge R262-D266 and a hydrogen bonding interaction between Y323-D289-Y293. In addition I288 interacts with hydrophobic interaction with a large buried surface area contributing significantly to dimer interface. The back-to-back dimer involves several residues within the helix αC. In addition, the other end of the helix αC contains

residues that co-ordinate the T446 within the active cleft. Therefore, there exists an allosteric link between the formation of the dimer interface and the activation of PKR. PKR is capable of dimerization in the absence of dsRNA and the K_d for self-associated was measured previously to be 500 μM[31]. Upon phosphorylation the affinity for dimerization increased by 1000 fold to ~ 500 nM.

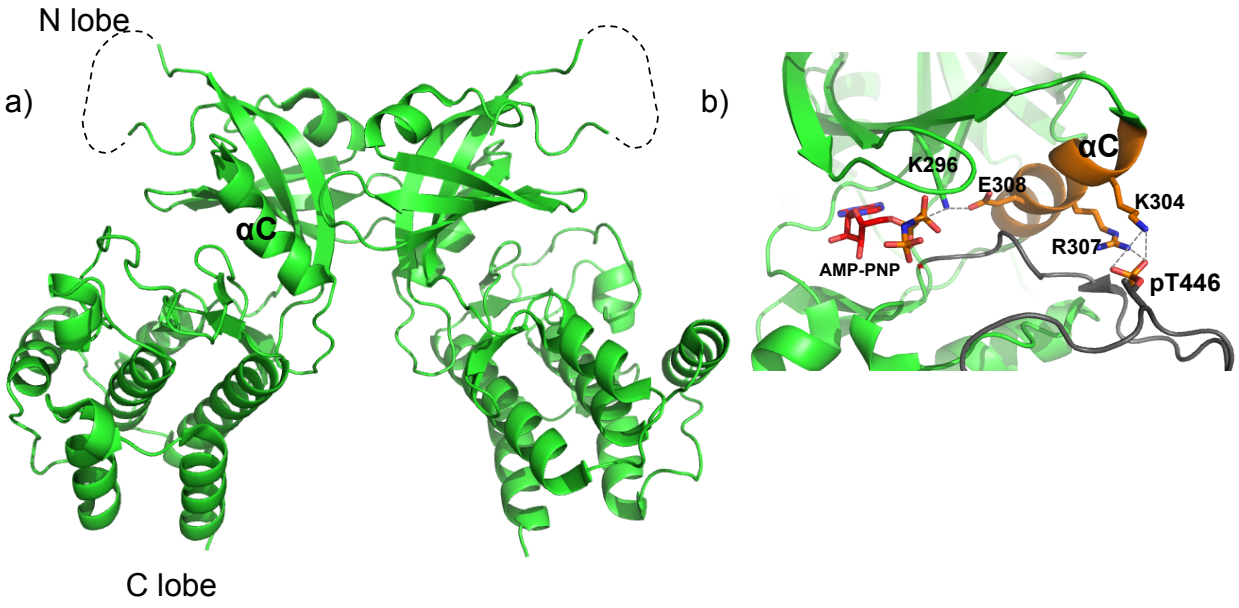

Figure 1.4. Allosteric linkage between dimerization and activation a) Back-to-back dimer of kinase b) Active site of kinase with AMP-PNP

1.5. Unstructured regions within PKR

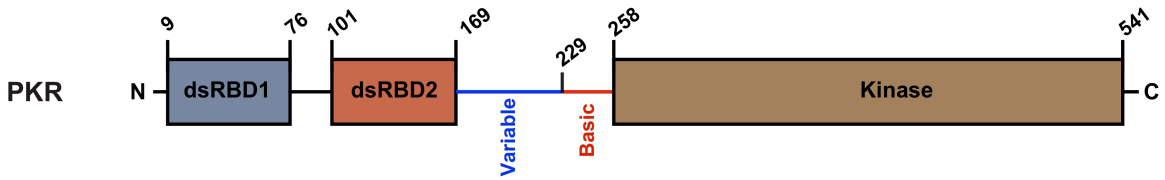

Figure 1.5. Inter-domain linkers of PKR.

Four of fifteen phosphorylation sites exist within the N-terminal region including threonine and serine residues in the linker region. One of the sites (S33) is located within dsRBD1 and may make contacts with dsRNA when bound. When PKR is autophosphorylated it has an enhanced affinity for dimerization and a reduced affinity for dsRNA. Therefore even a small amount of dsRNA can be recycled to initiate the activation of several PKR molecules. It is suggested that phosphorylation at S33 reduces the affinity for dsRNA and therefore is a critical site in the context of the autocatalytic cascade. The kinase domain is separated from the N-terminal region by a long unstructured linker. The linker contains only one phosphorylation site (S242) and alanine substitution at this site causes a slight attenuation of PKR activation potency but does not block activation[33]. The linker can be divided into two sections based on sequence homology and amino acid content. The region 169-229 is abundant in polar uncharged residues, which is a signature of disordered proteins. It is also interspersed with negatively charged residues (Figure 1.5.)[33]. The length of this sequence is variable across different homologs of PKR and is virtually absent in PKR from *Mesocricetus auratus* or golden Syrian hamster. The C-terminal region 229-258 is enriched in basic residues and may possess some α helical content as predicted by secondary structure

prediction algorithms. It is also relatively more conserved and contains the phosphorylation site at 242.

The 90 residue linker region between the dsRBD and the kinase domain of PKR is unstructured and is considered as an intrinsically disordered region based on full length PKR structural studies using SAXS[34] and NMR[35]. SAXS data obtained for PKR fit best to a model where the protein exists in an ensemble of open and closed states based on the end-to-end distance distributions. NMR studies with full length PKR have also shown that residues within the linker produce spectra that are characteristic of disordered proteins. There is some evidence to suggest that the linker may be involved in dsRNA independent activation associated with dimerization. Constructs of the kinase domain with the linker (169-551) were able to autophosphorylate at high concentrations while constructs of the isolated kinase domain (252-551) were unable to become activated at the same concentration range[35].

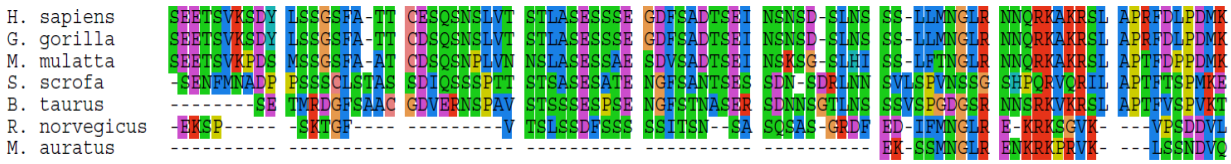

Fig. 1.6. Sequence alignment of the linker from eukaryotic homologs of PKR.

1.6 Objectives and goals

PKR is activated upon binding dsRNA by dimerization and autophosphorylation. The precise mechanism by which RNA binding stimulates activation is not clear. The active kinase forms a back-to-back dimer where the active sites are on opposite ends of the dimer. It is unclear how the autocatalytic pathway proceeds given the dimer

configuration. It was previously assumed that dsRNAs that were long enough to assemble more than one PKR monomer were activators. However certain RNAs can bind two PKRs without activating. It is difficult to test if activation is blocked by an inability to dimerize or by some other factor. Viral dsRNAs that interact with PKR *in vivo* possess relatively short duplex regions interrupted by complex secondary structural elements such as stem loops, internal loops and bulges. The mechanism by which PKR is able to interact across these RNA barriers and dimerize is unclear. The current methods available allow us to measure PKR assembly on dsRNA as well as activation. However, we cannot measure the interaction between adjacent kinases on a dsRNA. Formulating a protocol to measure PKR dimerization would allow us to confirm the dimerization model and to determine if dimerization is the only pre-requisite for activation.

1. **Define the modes of PKR binding to variable length duplex RNAs**.

Activation of PKR by longer dsRNAs is correlated with the interaction of the second dsRNA binding motif (dsRBM). Mutants of PKR that lack the ability of the dsRBM2 to bind dsRNA will be synthesized to investigate the role of this motif. The ability of the mutants to bind to variable length dsRNAs will be determined using analytical ultracentrifugation and PKR activation will be measured by autophosphorylation assays.

2. **Investigate the effect of RNA barriers on PKR dimerization and activation.**

RNA chimeras will be designed to contain two duplex PKR binding sites separated by variable length inert barriers such as 2'-O-methyl modified RNA. They will be used as molecular rulers to determine minimum barrier distance across which PKR can activate. The stoichiometry and affinity of PKR binding and PKR activation will be measured

using the techniques mentioned in Aim 1. The effect of other RNA barriers such as internal loops and mismatched pairs will also be determined.

3. Define the role of the unstructured linker in PKR dimerization.

The 90 residue linker may be involved in enabling the kinase domains to dimerize over barriers in dsRNAs such as internal loops and bulges. The ortholog of PKR from *Mesocricetus auratus* (golden Syrian hamster) has a much shorter linker of about 20 residues. Hamster PKR will be expressed and purified and its ability to interact with various length duplexes. In addition, linker-deleted constructs of human PKR will be characterized to test the effect of linker length on PKR activation. SAXS STUFF

4. Measure functional PKR dimerization using Förster resonance energy transfer (FRET)

Some dsRNAs are able to bind two PKR monomers but are incapable of activating PKR. We will directly assay dimerization of the kinase domain upon binding to activating and non-activating RNAs to determine whether dimerization is correlated with PKR activation. Fluorescent probes will be incorporated at specific sites near the PKR dimer interface by unnatural amino acid mutagenesis. FRET will be used to assay PKR kinase domain dimerization upon binding to RNAs. These studies will include the RNA chimeras and short duplexes mentioned in Aims 1 and 2.

2.1. Reagents, buffers and glassware

The buffer components and solvents used in the experiments were high purity reagent grade chemicals. Buffers were filtered using 0.22 µm membranes and autoclaved. TCEP was added to buffers immediately prior to use. Analytical ultracentrifugation cell components were sonicated and treated with RNAaseZap (ThermoFischer Scientific). Oligonucleotides used in the study were purchased from Dharmacon (Lafayette, CO).

Fluorescent dsRNA

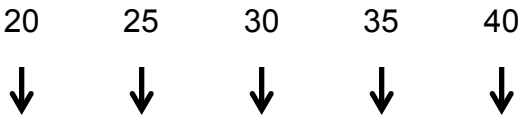

TS40F - 5'-**Fl** GGAGAACUUCAUGCCCUUCG GAUAA GGACU CGUAU GUACC-3'

BS40 - 3'- CCUCUUGAAGUACGGGAAGC CUAUU CCUGA GCAUA CAUGG-5'

Duplex dsRNA

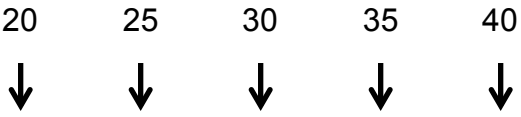

TS40B - 5'- GGAGGAUGUUAAUUGGCGUG UCUUG UCUGC AACGG UAUUC - 3'

BS40B - 3'- CCUCCUACAAUUAACCGCAC AGAAC AGACG UUGCC AUAAG - 5'

2'-O-Methyl dsRNA

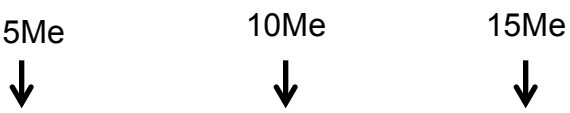

5' - GGAGGAUGUUAAUUG mGmCmGmUmG mUmCmUmUmG mUmGmUmCmA UCUGCAACGGUAUUC - 3'

Table 2.1. RNA sequences

RNA	Molecular weight (g/moles)	Mass extinction coefficient * (L/g*cm)
Fl20 bp	13062.1	4.78E6
Fl25 bp	16477.1	2.53E6
Fl30 bp	19699.0	3.39E6
Fl35 bp	22905.0	3.49E6
Fl40 bp	27655.1	2.49E6
20B bp	13793.0	22.31
30B bp	19142.0	24.66
40B bp	25718.8	23.86
15-5Me-15	22509.0	23.75
15-10Me-15	25855.2	21.24
15-15Me-15	29201.5	27.5

$$\textbf{*Mass extinction coefficient} = \frac{\textbf{Fluorescence or Absorbance intensity}}{[\textbf{RNA}]\ (\textbf{M}) * \textbf{path length}\ (\textbf{cm}) * \textbf{Molecular weight}\left(\frac{\textbf{g}}{\textbf{moles}}\right)} \quad \textbf{(1)}$$

2.2. Plasmids and site-directed mutagenesis

Single amino acid substitutions as well as deletions of human PKR were made using the pET-PKR/PPase vector. Hamster PKR was cloned into pET28a upstream of lambda phosphatase. Thermocycler from Biorad were used for all PCR reactions. All primers were designed and purchased from Integrated DNA Technologies (IDT). Phusion High Fidelity master mixes from New England Biolabs (NEB) were used for all PCR reaction

preparations. The pEVOL-pAzF vector used for the expression of p-azidophenylalanine (pAzF) specific amino-acyl tRNA synthetase (aaRS)/ $tRNA_{UAG}$ pairs was purchased from Addgene.

2.3. RNA purification

The strands were deprotected and purified using polyacrylamide gel electrophoresis. The RNA bands from the gels were cut and the RNA was extracted by electrolution (Elutrap, G.E. Whatman). The RNA was precipitated using 3.5 M sodium acetate/ 99% ethanol and dried using a Speed Vac centrifuge. The complementary strands were annealed at 80°C for 5 minutes in either AU200 (20 mM HEPES, 200 mM NaCl, 0.1 mM EDTA, pH 7.5) or AU75 (20 mM HEPES, 75 mM NaCl, 0.1 mM EDTA, pH 7.5) and slowly cooled to room temperature before use. The extinction coefficient of the duplex annealed strands was calculated and was usually ~10-25% lower than the sum of the extinction coefficient of the individual strands owing to hypochromism. Sedimentation velocity analysis was used to ensure that the dsRNAs were homogeneous.

2.4. Protein expression and purification

Human PKR constructs were transformed into Rosetta 2 pLyS cells and expressed as described previously[31]. Hamster PKR was expressed and purified differently due to reduced solubility. The pET-HamsterPKR/PPase vector was transformed into ArcticExpress RIL (DE3) cells which express cold shock proteins Cpn 60 and Cpn 10. Cells were grown at 37^{o}C until OD_{600} was ~0.8 and hamster PKR was induced at 10^{o}C for 16 hours. PKR constructs containing amber stop codon substitutions were co-transformed with p-EVOL-pAzF in ArcticExpress RIL (DE3) cells. Cultures were grown at 37^{o}C and 250 rpm. The aaRS/ $tRNA_{UAG}$ pair were induced at an OD_{600} of 0.2-0.3 with

0.02% arabinose. 1 mM pAzF (Bachem) was added 30 minutes after arabinose addition. All subsequent steps were performed in the dark under non-reducing conditions. 1 mM IPTG was added after cultures were cooled to 18^{o}C, and induction proceeded for four hours at room temperature. All PKR constructs were purified using a two-step purification protocol as described previously. Concentrated PKR fractions were separated from higher order aggregates by separation over size exclusion column (S-200/S-75, G.E. Life Sciences) in AU200 buffer (20 mM HEPES pH 7.5, 200 mM NaCl and 0.1 mM EDTA). Purified fractions were analyzed using SDS PAGE and concentrated using Amicon Ultracentrifugal filters (EMD Millipore)

2.5. Fluorescent labeling of pAzF-PKR

Purified pAzF-PKR was labeled with Alexa fluor 488 DIBO (Molecular Probes) or Cy3 DBCO (Click Chemistry Tools). 10 mM stocks of the dyes were prepared in 99% DMSO and stored at 4^{o}C. Labeling reactions contained 25 μM PKR and 70 μM dye in AU200 buffer with a reaction volumes of 500 μL. Reactions were incubated for 1.5 hours at room temperature and were quenched by buffer exchanging twice into AU200 containing 0.1 mM TCEP using spin columns containing P6 biogel beads (Biorad). The efficiency of labeling was measured by recording the absorbance at 280 nm and 495 nm or 553 nm for Alexa 488 or Cy3 respectively.

$$[\text{Dye}] = \frac{\text{Absorbance at 495 or 553 nm}}{\text{Extinction Coefficient of dye} * \text{path length}} \text{ (M)} \quad (2)$$

$$[\text{PKR}] = \frac{[\text{Absorbance at 280 nm} - (\text{Absorbance at 495 or 553} * \text{C.F.})]}{\text{Extinction Coefficient of PKR} * \text{path length}} \text{ (M)} \quad (3)$$

$$\text{Labeling Efficiency} = 100\% \text{ X } [\text{Dye}]/[\text{PKR}] \quad (4)$$

Where C.F. is the correction factor used to account for the contribution of the dye absorbance at 280 nm. The C.F. for Alexa 488 is 0.11 and is 0.08 for Cy3. The extinction coefficients used for human PKR, Alexa 488 and Cy3 were 43,400 M^{-1} cm^{-1}, 71,000 M^{-1} cm^{-1} and 151,000 M^{-1} cm^{-1} respectively.

2.6. Sedimentation velocity experiments with PKR and dsRNAs

Absorbance detected sedimentation velocity analysis of PKR-dsRNA interactions was performed in AU200 buffer at 20°C using absorbance optics at 260 nm as previously described[36]. Fluorescence sedimentation velocity experiments were performed using a Beckman-Coulter XL-I analytical ultracentrifuge equipped with an AU-FDS Fluorescence detector (AVIV Biomedical, Lakewood, NJ) at 20°C and 40,000 rpm unless specified. Samples contained 20-30 nM dsRNA and varying concentrations of PKR in either AU200 or AU75 buffer were loaded into double sector cells equipped with 1.2 cm Spin60 charcoal-epon centerpieces (Spin Analytical, Berwick, ME) and quartz windows. During a pre-run at 5,000 RPM the photomultiplier voltage and gain multiplier settings were adjusted to give ~ 3000 counts and the focus depth was set to give a maximum signal. Absorbance intensity scans were recorded for each channel following the sedimentation velocity experiment and the meniscus position was determined from a characteristic downward intensity spike.

The protein partial specific volume and the buffer densities and viscosities were calculated using SEDNTERP. The partial specific volumes of the dsRNAs were fixed at 0.55 ml g^{-1}. The sedimentation velocity data for the dsRNAs were first analyzed using a c(s) distribution model with Sedfit to ensure that the preparations were homogenous and free of contaminants. The data were then fit to a single species model to obtain the

sedimentation coefficients and the buoyant molar masses that were then fixed in subsequent global analyses of PKR binding. Sedimentation velocity analyses of PKR-dsRNA interactions were performed as previously described with some modifications to accommodate fluorescence data as described below. Initially, the data were analyzed using the time derivative method with DCDT+ to obtain g(s*) distributions to define the interaction model. Model-dependence global analysis was performed using SEDANAL to define the association constants and sedimentation coefficients of the protein-RNA complexes. For data acquired with the fluorescence detector, the amplitude of the stochastic noise depends strongly on the signal intensity. Therefore, the curve fits were weighted by the standard deviation at each point. This also served to convert the RMSD reported by SEDANAL from arbitrary fluorescence intensity units to χ, where a value of 1.0 corresponds to a perfect fit. Joint confidence intervals were obtained using the F-statistic to define a statistically significant increase in the variance.

2.6. Sedimentation equilibrium analysis of PKR

Sedimentation equilibrium analysis of PKR self-association was performed in AU200 at 20°C or 4°C as indicated using Rayleigh interference optics. Six-channel external loading cells were used at rotor speeds of 18,000, 22,000, 28,000 rpm. Scans of water blanks were collected at each speed prior to running PKR samples. The blank scans were subtracted from the samples and data were analyzed using HETEROANALYSIS[37].

2.7. PKR activation

Quantitative phosphorylation assays were carried out as previously described by incubating 200 nM PKR with varying concentrations of dsRNA in AU75 buffer containing 5 mM MgCl2 and 0.1mM TCEP at 32 °C for 20 minutes. The phosphorylation reactions were initiated with 0.4 mM ATP containing 4 μCi [γ-32P] ATP in each reaction mixture and were quenched after 20 minutes by adding SDS sample loading buffer unless indicated otherwise. The reaction mixtures were then heated to 90 °C for 3 minutes and were analyzed using SDS PAGE electrophoresis and phosphor imaging (Typhoon, GE Healthcare).

2.8. Steady state fluorescence anisotropy measurements

Steady state fluorescence anisotropy and emission measurements were recorded with a FluoroMax-3 fluorimeter equipped with Glan-Thompson polarizers (Jobin Yvon Inc., New Jersey). All measurements were performed at 20°C with samples in either AU200 or AU75 buffer using a 10 mm path length quartz cuvette (Precision Cells).

Fluorescence anisotropy measurements were performed with Alexa 488-labeled PKR at excitation and emission wavelengths of 495 nm and 518 nm and bandwidths of 2 and 3 nm, respectively. Intensities were integrated at each polarization for 5 s with three repetitions. The data were corrected for buffer background and the anisotropy (r) was calculated as

$$r = \frac{I_{\parallel} - GI_{\perp}}{I_{\parallel} + 2GI_{\perp}} \tag{4}$$

where $I_{\parallel}$ and $I_{\perp}$ correspond to the fluorescence intensity with the excitation polarizer oriented in the vertical position and the emission polarizer in the vertical and horizontal

positions, respectively. The G factor corrects for instrument polarization bias and was measured to be ~0.64.

In a cluster of identical molecules undergoing Homo-FRET, the emission is the sum of the contribution of the initially excited chromophore and the other chromophores. Energy transfer-induced depolarization of the emission and several expressions have been derived for the steady state anisotropy expected for a dimeric cluster. The results are very similar; here, we use the formalism of Runnels and Scarlatta.

The total anisotropy of the dimeric cluster (r_{tot}) is the sum of the anisotropy of the initially excited chromophore (r_1) and the anisotropy of the molecule excited by energy transfer (r_{et})[38]

$$r_{tot} = r_1 \frac{1+\left(R_0/R\right)^6}{1+2\left(R_0/R\right)^6} + r_{ET} \frac{\left(R_0 R\right)^6}{1+2\left(R_0 R\right)^6} \quad (5)$$

where R_0 is the Förster distance and R is the distance between the chromophores. In the case of a dimeric cluster with random relative orientation of the chromophores, energy transfer results in complete depolarization such that $r_{et} = 0$. Even in the case of rigid, parallel emission and excitation dipoles, r_{et} is only 0.016. For pAzF261-A488 r_1 = 0.2869, and for the PKR dimer in the back-to-back, antiparallel orientation, R = 25 *Å* (Figure 1B). R_0 for Alexa Fluor 488 self-transfer is 48 *Å*[39] and equation S1 (assuming r_{et}=0) predicts r_{tot} = 0.145, or about half the monomer value. An antiparallel PKR dimer model was constructed by aligning the PKR kinase (PDB accession 2A1A) onto the GNC2 dimer structure (PDB accession 1ZYC) using interface residues conserved

between PKR and GCN2. In this case, the inter-chromophore distance increases to R = 49 *Å* and r_{tot} = 0.195, or about 2/3 of the monomer.

2.9. Small angle X-Ray scattering (SAXS) of ΔV PKR

SAXS measurements were performed in AU200 buffer at 4^{o}C using a Nanostar instrument (Bruker, Madison, WI) equipped with a rotatating anode source and 550 μm scatterless pinholes. Proteins were centrifuged at 14,000 rpm for 10 minutes prior to measurements. Data were collected in four 1 h frames at a sample-detector distance of 67.2 cm proving a range of q = 0.007- 0.37 Å^{-1}. Data were reduced using Bruker SAXS software. The four scans overlayed, indicating the absence of radiation damage. Buffer background scattering (15 1 hour frames) was subtracted from the data prior to analysis. Guinier analysis was performed using the low-q portion of the data where R_g•q<1.3. The p(r) distributions were produced using GNOM and the maximum dimension (D_{max}) was manually adjusted to the distance where the p(r) distribution approaches zero. Structural modeling was performing using EOM 2.0. The program generated a pool of 10,000 possible scattering intensities using the Ranch software. Then a genetic algorithm was applied to obtain a distribution which represents the ensemble that fit best to the experimentally obtained scattering curve for the protein. The ensemble distribution was for a default set of curves as decided by the algorithm.

Chapter 3: Effect of salt concentration on PKR-dsRNAs binding

3.1. Introduction

Protein kinase R (PKR) is an important component of the interferon-induced innate immune pathway[3]. PKR is synthesized in the cell in a latent, unphosphorylated form and becomes activated and undergoes autophosphorylation upon binding to certain host or pathogen associated RNAs or upon interacting with the protein PACT. Activated PKR phosphorylates eukaryotic Initiation Factor 2α (eIF2α), causing an inhibition of protein synthesis. Many viruses have developed mechanisms to inhibit PKR[40].

PKR contains an N-terminal dsRNA binding domain and a C-terminal kinase domain, separated by a flexible linker region. The N-terminal dsRNA binding domain (dsRBD) corresponds to the regulatory domain which consists of two tandem copies of the dsRNA binding motif, dsRBM1 and dsRBM2. This motif binds duplex RNA in a non-sequence specific manner but discriminates against ssRNA and dsDNA[41]. Each motif adopts the conserved $\alpha\beta\beta\beta\alpha$[18] fold and they are separated by an unstructured linker of ~20 amino acids. The crystal structure of a dsRNA-binding domain complexed with dsRNA reveals a[3] site size of 16 bp[11]. The C-terminal kinase domain is the catalytic center. The crystal structure of the PKR kinase domain in complex with eIF2α reveals that the catalytic center has the canonical protein kinase fold. The complex forms a dimer where the interface is in the N-terminal lobe of the kinase domain[17].

PKR is regulated by a variety of cellular and viral RNAs that contain duplex regions[42]. The most well characterized activators of PKR are simple dsRNAs. There is strong evidence that dimerization plays a crucial role in the mechanism of PKR

activation by dsRNA[5,43]. Latent PKR dimerizes weakly in solution but this reaction is sufficient to activate PKR in the absence of RNA[31]. An allosteric pathway has been identified that couples the dimer interface with the kinase active site and dimer interface mutations can modulate PKR activation[17,44]. A hallmark of PKR activation by dsRNA is the "bell-shaped" curve where low RNA concentrations activate but higher concentrations are inhibitory[12,15]. These observations support a model in which multiple PKRs assemble on a single dsRNA and high dsRNA concentrations dilute PKR monomers onto separate molecules of dsRNA[45]. In the context of regular duplex RNA, a minimum of 30-33 bp of dsRNA are required to activate PKR autophosphorylation and the maximal level of activation increases with duplex length[12,13]. .

The mechanism of assembly of PKR on duplex RNAs has been extensively investigated. PKR can bind to duplexes as short as 16-18 bp[19,20]. As expected for a non-sequence specific interaction, the binding stoichiometry increases with dsRNA length[12,13,19,20]. The binding stoichiometries for the dsRBM1 and for a construct containing dsRBM1 and dsRBM2 are greater than predicted from the site size[20,46]. Based on these results, we proposed an overlapping ligand binding model where the motif binds to multiple faces of the dsRNA duplex and overlaps along the helical axis. The increase in binding affinity with increasing dsRNA length can be understood as a statistical consequence of the greater number of configurations available on the longer lattice. The intrinsic binding affinities of a dsRBM1-dsRBM2 construct and full length PKR for a 20 bp RNA are similar[13,20] but the stoichiometries are lower for the latter. A minimum of 30 bp of dsRNA are required to bind two full length PKR monomers with high affinity, which correlates with the minimal dsRNA capable of activating through

autophosphorylation. Binding affinities increase dramatically upon reducing the salt concentration from 200 to 75 mM NaCl and a second PKR can bind to 20 bp duplex at lower salt[13].

The non-sequence specific interactions of PKR with RNAs are labile and it is important to use solution biophysical methods to accurately measure the binding parameters at thermodynamic equilibrium. Our previous analyses of PKR binding to dsRNA by sedimentation velocity analytical ultracentrifugation[13,31] were limited by formation of nonspecific aggregates, even at the minimal RNA concentrations required for detection using absorption optics. Aggregation is enhanced for longer RNAs and at lower salt concentrations. In addition, it is difficult to quantify high affinity binding constants due to the limited sensitivity of the absorbance optics. Here, we have used fluorescence detection of labeled dsRNAs to enhance the sensitivity of sedimentation velocity measurements and directly characterize the interaction of PKR with duplex RNAs ranging from 20-40 bp and at multiple salt concentrations. The binding affinities increase at lower salt concentration and with longer dsRNA length, and in some cases the stoichiometries of binding of PKR to dsRNA increase at 75 mM NaCl. The dependence of the binding stoichiometries on dsRNA length does not conform to standard statistical models for nonspecific binding. We propose a model where the activation of PKR by longer RNAs is correlated with an alternative binding mode that allows for direct interaction of the kinase domains.

3.2. Results

3.2.1. Sedimentation velocity of PKR and various length duplexes

The enhanced sensitivity of fluorescence detection in sedimentation velocity measurements allows the dsRNA concentrations to be greatly reduced, from ~1 μM using absorbance detection at 260 nm to 20-30 nM for fluorescence analysis of 5'-fluorescein labeled RNAs. Figure 3.1. shows an analysis of PKR binding to dsRNA using a long sequence (40 bp) at low salt (75 mM NaCl), conditions that previously were found to promote aggregation. The signal/noise of the raw sedimentation velocity traces for the RNA alone is excellent (Figure 3.1.A). The data fit well to a model of a single species with a corrected sedimentation coefficient of $s_{20,w}$ = 3.69 S and a molecular weight of 30,979 g/mol consistent with a predicted mass of 26,128 g/mol based on the RNA sequence. Thus, this dsRNA preparation is homogenous and suitable for analysis of PKR binding.

The binding of PKR to the 40 bp dsRNA was characterized by a sedimentation velocity titration using fluorescence detection. Although the general approach is similar to the method we have previously described by analysis of PKR-RNA interactions using absorbance detection[36], the RNA concentration here is much lower and we are able to access a much broader range of PKR concentrations, ranging from nM to μM. Another difference is that the PKR contributes, albeit weakly, to the absorbance signal measured at 260 nm whereas only the fluorescein-labeled RNA contributes to the fluorescence signal.

Initially, the velocity data are analyzed using a model-independent approach to help define the correct binding mode. Figure 3.1.B shows a titration of the 40 bp dsRNA over

a broad range of PKR concentration from 50 nM to 7 μM, represented as an overlay of normalized g(s*) sedimentation coefficient distributions. The formation of PKR-dsRNA complexes causes the distributions to shift far to the right, to a saturating value of ~ 9.46 S at 2 μM PKR. Hydrodynamic calculations indicate that the magnitude of this shift is greater than expected for binding of a single PKR but is consistent with binding of three PKR monomers (Table 3.2.). The g(s*) distribution at 7 μM exhibits a shoulder at higher S, indicating formation of higher aggregates. However, the data obtained over the range 50 nM - 2 μM can be globally fit to a sequential binding model to resolve the three equilibrium constants (Figure 3.1.C). The fit is of good quality, with small systematic deviations in the residuals and RMSD = 1.70. As we have previously observed for PKR binding to dsRNA lattices[13,20,46], the first PKR binds most strongly, with K_{d1} ~30 nM and the second and third ligand bind progressively more weakly, with K_{d2} ~ 50 nM and K_{d3} ~ 250 nM Table 3.1.). Note that these are stepwise, macroscopic dissociation constants and are not corrected for statistical effects. Fitted values for the sedimentation coefficients of the three complexes RNA-PKR, RNA-PKR_2 and RNA-PKR_3 (Table 3.2.) correspond to frictional ratios of 1.42, 1.46, and 1.40, respectively, which lie in the range typically observed for RNA-PKR complexes[36].

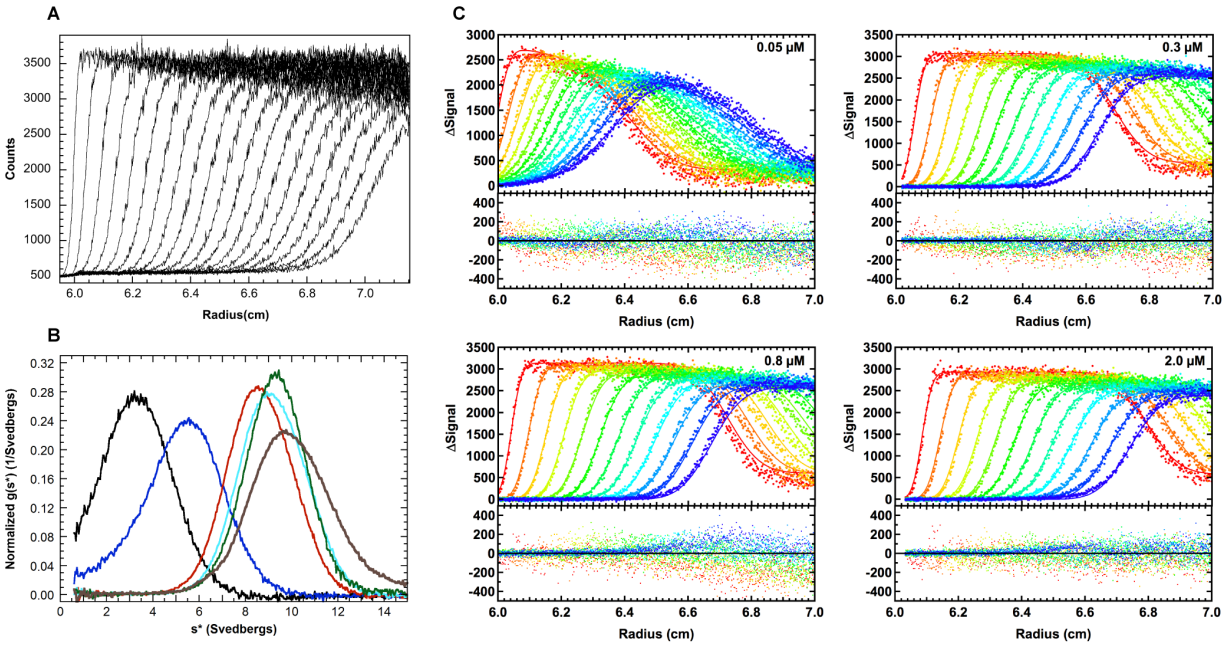

Figure 3.1. Sedimentation velocity analysis of PKR binding to a 40 bp dsRNA in AU75. (A) Raw sedimentation velocity profiles for 40 bp dsRNA. For clarity, only every 13th scan is shown. (B) Normalized g(s*) distributions of 0.03 μM 40 bp dsRNA (black), dsRNA + 0.05 μM PKR (blue), dsRNA + 0.3 μM PKR (red), dsRNA + 0.8 μM PKR (cyan), dsRNA + 2 μM PKR (green), dsRNA + 7 μM PKR (brown). (C) Global analysis of difference curves. The data were subtracted in pairs to remove systematic noise and the four data sets at the PKR concentrations were fit to a 2:1 binding model using SEDANAL. The top panels show the data (points) and fit (solid lines) and the bottom panels show the residuals (points). The best-fit parameters are shown in Table 3.1. For clarity, only every 7th difference curve of the 165 scans that were fit is shown.

Table 3.1. PKR-dsRNA dissociation constants measured in AU75 and AU200 buffers at 20°C.

dsRNA (bp)	[NaCl] mM	Model [a]	K_{d1} (nM)	K_{d2} (nM)	K_{d3} (nM)	RMSD [b]
20	75	2	45.2 (35.2, 59.5)	54.1 (40.9, 69.9)	-	1.54
20	200	1	303 (263, 349)	-	-	1.50
25	75	2	7.8 (6.8, 9.0)	473 (391, 572)	-	1.83
25	200	1	438 (380, 497)	-	-	1.27
30	75	2	100.1 (83.1, 122.5)	22.6 (18.6, 26.8)	-	1.54
30	200	2	52.0 (46.0, 58.3)	6270 (3920, 11800)	-	1.31
35	75	2	7.6 (6.7, 8.6)	69.1 (50.8, 95.2)	-	1.67
35	200	2	61.1 (47.9, 72.8)	4910 (2950, 8260)		1.38
40	75	3	32.1 (27.3, 38.0)	52.4 (40.6, 67.8)	245 (212, 280)	1.70
40	200	2	38.1 (29.5, 47.3)	813 (645, 1070)	-	1.52

Parameters were obtained by global nonlinear least square analysis of sedimentation velocity experiments. The values in parentheses represent the 95% joint confidence intervals obtained using the F-statistic.

[a]The model is specified by the stoichiometry of PKR binding.

[b] The root mean square deviation of the fit. Because the fits were weighted by the standard deviation of the data at each point, a perfect fit corresponds to an RMSD of unity.

Table 3.2: Hydrodynamic parameters for dsRNAs and dsRNA-PKR complexes.

dsRNA (bp)	PKR:dsRNA[a]	[NaCl] mM	Molecular Mass (g/mol)	s (S)	$s_{20,w}$ (S)	f/f_o
20	0:1	75	13285.2	2.42	2.48	1.58
20	1:1	200	75380.2	4.73	5.00	1.39
20	1:1	75	75380.2	4.83[b]	5.00	1.39
20	2:1	75	137475.2	6.26	6.47	1.61
25	0:1	75	16474.1	2.79	2.86	1.67
25	1:1	200	78569.1	4.80	5.07	1.53
25	1:1	75	78569.1	4.91[b]	5.07	1.53
25	2:1	75	140664.1	6.79	7.02	1.53
30	0:1	75	19699	3.05	3.12	1.72
30	1:1	200	81794.0	5.22	5.51	1.47
30	1:1	75	81794.0	5.33[b]	5.51	1.47
30	2:1	200	143889.0	7.49	7.92	1.39
30	2:1	75	143889.0	7.68	8.02	1.39
35	0:1	75	22905.9	3.27	3.36	1.75
35	1:1	200	85000.9	5.81	6.12	1.38
35	1:1	75	85000.9	5.93[b]	6.12	1.38
35	2:1	200	147095.9	7.32	7.73	1.47
35	2:1	75	147095.9	8.22	8.49	1.33
40	0:1	75	26127.9	3.59	3.69	1.76
40	1:1	200	88222.9	5.97	6.29	1.42
40	1:1	75	88222.9	6.03[b]	6.29	1.42
40	2:1	200	150317.9	7.65	8.08	1.46
40	2:1	75	150317.9	7.73[b]	8.08	1.46
40	3:1	75	212412.9	9.77	10.10	1.40

[a] The ratio of PKR to dsRNA in each complex.

[b] The sedimentation coefficient in AU75 could not be obtained from global analysis in SEDANAL and was fixed based on the corresponding value obtained in AU200.

These results obtained with the 40 bp dsRNA in AU75 demonstrate that it is feasible to analyze PKR binding to relatively long dsRNAs, even at low ionic strength, by reducing the dsRNA concentration into the nM range using the high sensitivity afforded by fluorescence detected analytical ultracentrifugation. We have employed this approach to rigorously define the PKR binding stoichiometries and affinities for a truncation series of dsRNAs ranging from 20 to 40 bp in 5 bp increments. Binding parameters were obtained at both high (200 mM) and low (75 mM) concentrations of NaCl. As described above for the 40 bp duplex, the binding stoichiometries were based on the limiting sedimentation coefficients estimated from the shift in g(s*) distributions with increasing PKR concentration. The models were verified and binding constants were resolved by global analysis of the data using SEDANAL. For the measurements performed in 75 mM NaCl, where the binding affinity is high, it was not possible to reliably fit for the sedimentation coefficients of the intermediate dsRNA-PKR complexes due to low population of these species. The sedimentation coefficients for these species were fixed at the values obtained in 200 mM NaCl (corrected for buffer density and viscosity). The results of the fits are summarized in Table 3.1. and the corresponding hydrodynamic parameters are presented in Table 3.2.

There are several trends that emerge from the analysis of PKR binding to the RNA truncation series at high- and low-salt conditions. For several of the dsRNAs (20, 25 and 40bp) the apparent binding stoichiometries increase at lower salt. This effect is likely associated with the enhancement in binding affinity that occurs at lower salt[19]. The K_ds decrease by as much as 10-fold upon reducing [NaCl] from 200 to 75 mM. Thus, the second (20 and 25 bp) or third (40 bp) PKR is not detectable at high salt because K_d

becomes too high. In most cases, the dissociation constants sequentially increase such that $Kd_1<Kd_2<Kd_3$. This successive decrease in binding affinities is not due to a negative cooperativity but represents a statistical effect. The macroscopic, stepwise binding constants measured in sedimentation velocity experiments correspond to the product of an intrinsic binding constant k and a statistical factor corresponding to the number of microscopic configurations of the ligand on the dsRNA[46,47]. As the RNA is sequentially saturated with ligand the statistical factors decrease, resulting in successively weaker binding. As expected for a nonspecific protein-nucleic acid interaction, the limiting binding stoichiometries measured in AU75 increase with the length of the dsRNA. However, this trend is surprisingly weak: upon doubling the lattice length from 20 to 40 bp the number of PKRs that bind does not double and only increases from 2 to 3.

3.2.2. Activation of PKR by duplexes in low salt

It has previously been reported that activation of PKR requires a minimum of 30 bp of dsRNA[12] and we have correlated PKR activation with the stoichiometry of binding measured in AU200 buffer for the dsRNA truncation series[13]. Our PKR binding data indicate a strong dependence of binding stoichiometry on salt concentration. Thus, we have re-examined the dependence of PKR activation of dsRNA length in a lower salt, AU75 buffer (Figure 3.2.). The activation profiles are very similar to those we previously observed at higher salt. A minimum of 30 bp are required to detect activation with a maximum near 30 nM and the maximal extent of activation increases with the length of the dsRNA. Thus, although the 20 and 25 bp dsRNAs can each bind two PKRs in

AU75 buffer, they are incapable of stimulating autophosphorylation under the same conditions.

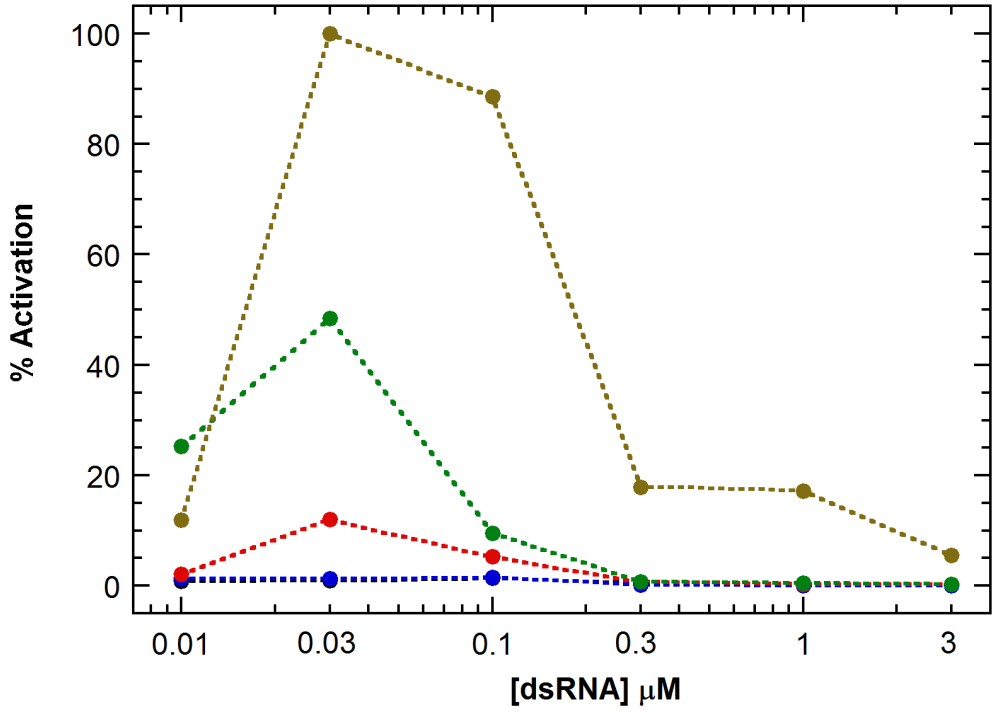

Figure 3.2. Activation of PKR by varying length duplex RNAs in 75 mM NaCl. Experiments were performed as previously described (*10*) in AU75 buffer at 32°C. Each reaction contains 200 nM PKR, 0.4 mM ATP, 4 μCi [γ-^{32}P]-ATP and the indicated amount of RNA. The reaction was allowed to proceed for 20 min at 32°C before quenching with SDS loading buffer and resolved on SDS-PAGE. 20bp dsRNA (black), 25bp dsRNA (blue), 30bp dsRNA (red), 35bp dsRNA (green), 40bp dsRNA (brown)

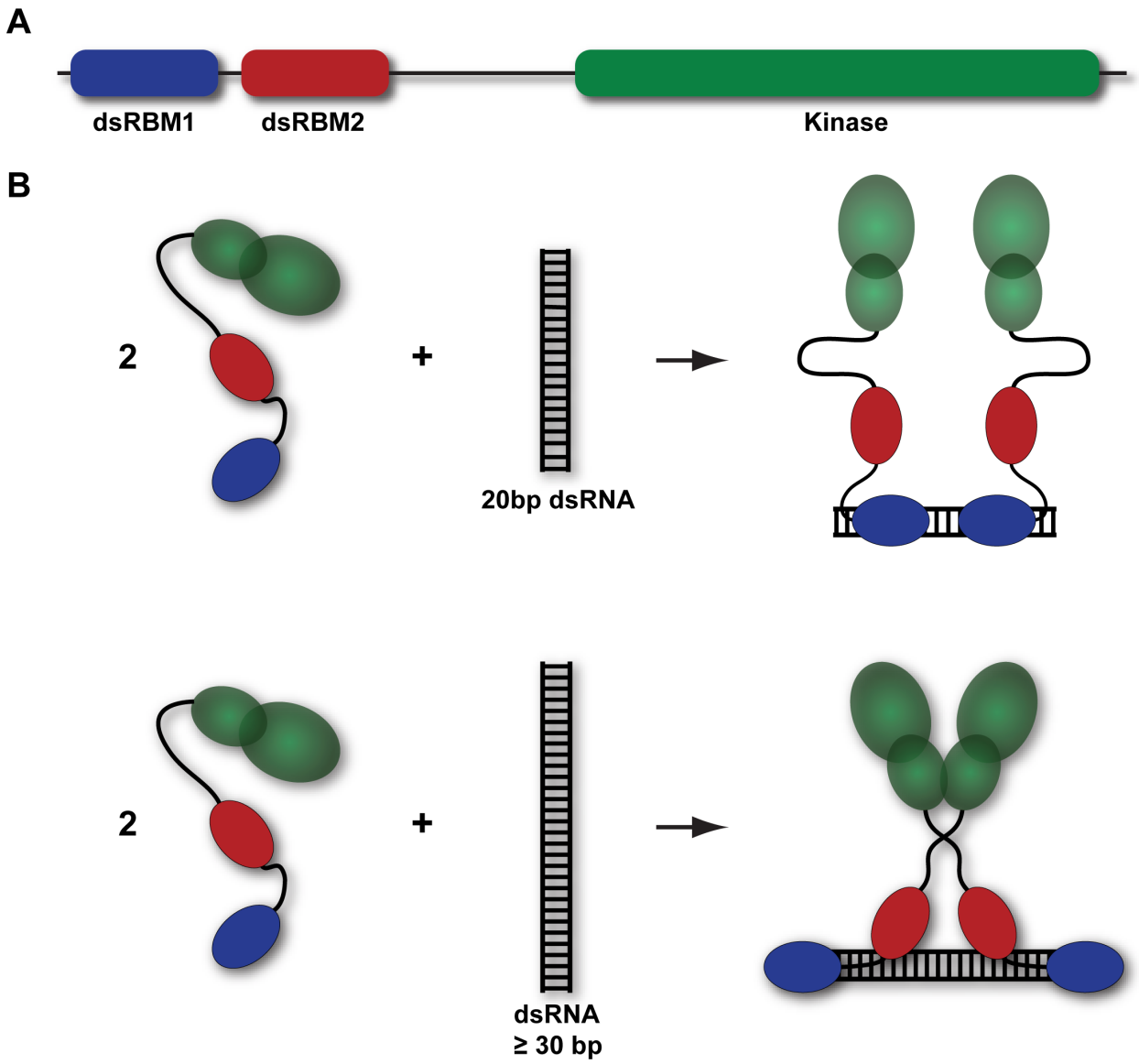

Figure 3.3. Model for PKR binding to short and long dsRNAs. (A) Domain organization of PKR. (B) Two PKRs are able to bind to the 20 bp dsRNA at low salt via dsRBM1. PKR binds to dsRNAs of ≥ 30 bp with a larger site size via interaction of both dsRBM1 and dsRBM2. This binding model facilitates dimerization of the kinase domains, resulting in PKR activation.

Discussion

The enhanced sensitivity afforded using fluorescein-tagged dsRNAs with fluorescence-detected analytical ultracentrifugation has allowed to us greatly reduce RNA concentrations from micromolar to nanomolar. In contrast to previous studies of PKR-dsRNA interactions by analytical ultracentrifugation[13], at lower RNA concentrations the analysis of binding stoichiometries and affinities is not complicated by aggregation formation and we were able to directly characterize the interaction of PKR with duplex RNAs ranging from 20-40 bp at multiple salt concentrations. The binding stoichiometries obtained here at 200 mM NaCl agree with those obtained earlier except for the 40 bp dsRNA, where we previously detected three PKR ligands by fluorescence anisotropy and sedimentation equilibrium[13] but only two in the present sedimentation velocity measurements. Note that sedimentation velocity has greater resolving power than the earlier techniques and small amounts of aggregate may have contributed to a higher apparent stoichiometry. The dissociation constants for the 20 and 30 bp dsRNAs in 200 mM NaCl differ slightly from those previously obtained using absorbance detection. The origin of the discrepancies is not clear but the broader PKR concentration range used for the present experiments make them more reliable.

The dependence of the PKR binding stoichiometries and affinities on salt concentration and RNA length provides insight into the mechanism of assembly of PKR on duplex RNAs and formation of active complexes. There is a large electrostatic component to the PKR-dsRNA interaction[19] that results in increased binding affinity as the NaCl concentration is decreased from 200 to 75 mM. The concomitant increase in binding stoichiometries for several of the RNAs is likely associated with the

enhancement in binding affinity. Limited solubility of PKR-RNA complexes precludes measurements at NaCl concentrations below 75 mM and we make the assumption that the stoichiometries measured under these conditions correspond to the maximum. We have previously characterized the binding of the PKR dsRBD, containing both dsRBM1 and dsRBM2, and dsRBM1 alone to the same dsRNA truncation series in AU75 buffer[20,46]. The stoichiometries for the full-length enzyme are consistently lower for either domain construct across the range of RNA lengths. Presumably, the presence of the kinase domain and linker in PKR result in steric hindrance, which increases the effective binding site size relative to the domain constructs.

The dependence of the limiting PKR binding stoichiometries on dsRNA length does not conform to standard models for nonspecific binding of proteins to finite nucleic acid lattices[48-50]. The stoichiometries are expected to regularly increase with RNA length, but for PKR they remain fixed at 2 PKR/RNA from 20-35 bp and only increase to 3 for the 40 bp sequence. In contrast, the stoichiometries for dsRBM1 binding to RNA increase strongly with length and conforms to a modified overlapping ligand binding model[46] where the motif binds to multiple faces of the dsRNA duplex and overlaps along the helical axis with a site size of 12 bp and a minimum overlap of 4 bp[20]. The dsRBD also follows this model for RNAs up to a length of 30 bp but deviates strongly for longer RNAs, and the stoichiometries actually decrease between 35 and 40 bp. These data indicate a change in binding mode to a larger size with increasing RNA length. This model is supported by NMR mapping experiments showing that only the N-terminus of dsRBM2 interacts with a 20 bp dsRNA but extensive interactions are observed upon binding to the 40 bp sequence[20]. In addition, affinity cleavage experiments demonstrate

that simultaneous binding of both dsRBMs of PKR is correlated with PKR activation[51]. We suggest that an analogous change of binding mode occurs as a function of RNA length for the full-length enzyme, resulting in an increase in the site size and a constant binding stoichiometry from 20-35 bp.

Although dimerization clearly plays a critical role in the PKR mechanism[43], the ability of a single dsRNA to bind 2 PKR monomers is not sufficient to induce autophosphorylation. In AU75 buffer the 20 and 25 bp RNAs each bind 2 PKRs yet are incapable of inducing measurable autophosphorylation (Figure 3.2.). Previously, we suggested that the inability of these shorter RNAs to activate in AU200 is associated with low binding affinities, resulting in low population of the active $(PKR)_2$:RNA species[13]. However, the 20 and 25 bp RNAs also do not activate in AU75, yet the binding affinities measured in this buffer are as strong as those measured for a 30 bp RNA in AU200 where this RNA is capable of activating PKR autophosphorylation. Thus, additional factors must be limiting the ability of short RNAs to induce the functional, active dimeric form of PKR. We propose that activation of PKR by longer RNAs requires a binding mode that inaccessible upon binding to shorter RNAs (Figure 3.3.). Our RNA binding data indicate that this active binding state is characterized by a larger size. Possibly, this mode is required to allow for direct interaction of the kinase domains to mediate functional dimerization.

Chapter 4: Assaying PKR dimerization

4.1. Introduction

The N-terminal regulatory module of PKR consists of two dsRNA binding domains (dsRBDs)[18]. Although the PKR dsRBDs bind dsRNA without sequence specificity[19], there is evidence for shape recognition and sequence readout in the minor groove in some other dsRBDs[52]. The catalytic domain has the typical bilobal architecture found in protein kinases, consisting of a smaller N terminal (N-) lobe and a larger C terminal (C-) lobe[17].

A key mechanistic issue is how interaction of the PKR dsRBDs with dsRNA leads to activation of the kinase. Early studies supported an autoinhibition model in which the latent form of PKR is locked in a closed conformation where the second dsRBD interacts with the kinase and blocks substrate binding[43]. In this scenario, RNA binding to the dsRBDs leads to an open, active state. This view is supported by NMR chemical shift perturbation measurements that reveal interaction between the second dsRBD and the kinase[53,54]. However, this interaction is extremely weak (K_d ~ 250 μM)[55]. SAXS[34], AFM[56] and NMR[35] analysis of latent PKR reveal that the long (~90 amino acid) linker between the dsRBDs and the kinase domain is flexible and unstructured, giving rise to a range of open and closed conformations that is inconsistent with the autoinhibition model.

An emerging mechanism in the regulation of protein kinases is the allosteric linkage of dimerization with a conformational transition to an active state[57]. Structural and biophysical analyses support a pivotal role for dimerization in activation[43]. The PKR

kinase domain forms a dimer in both active, phosphorylated[17] and inactive state[58]. PKR dimerizes only weakly (K_d ~ 500 μM); however, this reaction is sufficient to activate autophosphorylation in the absence of dsRNA[31]. In the context of duplex RNA, the minimum length of ~30bp of duplex required to activate PKR [12,13]correlates with the minimum length capable of binding two PKR monomers with high affinity[59]. PKR activation exhibits a characteristic bell-shaped curve where high dsRNA concentrations inhibit[12], consistent with a model where PKR dimers are dissociated by dilution onto separate dsRNAs[45]. These results support a PKR activation model where RNA binding functions to bring two kinase domains into close proximity and facilitate dimerization.

Dimerization plays a role in the activation of other eIF2α kinases. PERK dimerization is linked to activation[60] whereas HRI[61] and GCN2[62] exist as constitutive dimers. The structure of a phosphorylated PERK kinase domain reveals a back-to-back parallel dimer similar to PKR[63]. Although a similar N-lobe dimer interface is observed in a structure of an unphosphorylated GCN2 kinase domain, it adopts a novel, antiparallel orientation where one subunit is rotated approximately 180°[64]. Interdimer hydrogen bonding (Y323-D289) and salt-bridge (R262-D266) residues are conserved within the family. Mutations designed to disrupt the salt-bridge in PKR, GCN2 and PERK block kinase activity and charge reversal restores biological function[44,65,66]. This contact is formed in the parallel PERK dimer, but the corresponding residues are too far apart in the antiparallel GCN2 dimer to form a salt bridge. The antiparallel GCN2 dimer likely corresponds to an inactive conformation and activation may be associated with rotation to a parallel structure that results in formation of the essential salt-bridge[57,64].

Interestingly, simultaneous binding of two or more PKRs to an RNA does not necessarily activate. For example, at low salt two PKRs can bind RNAs as short as 20 bp without inducing autophosphorylation[59]. Typical protein-RNA interaction measurements can count the number of protein monomers bound to an RNA but cannot determine whether the proteins directly interact on the RNA to form a dimer. Thus, we have developed a sensitive fluorescence assay to direct probe the role of PKR kinase domain dimerization in RNA-induced activation. We observe efficient dimerization upon binding to activating duplex RNAs. Surprisingly, several non-activating RNAs that bind multiple PKRs also induce dimerization. We propose that PKR can adopt an alternative, non-activating dimer configuration.

4.2. Results

4.2.1. Characterization of *p*AzF-261-A488

A homo-Förster Resonance Energy Transfer (homo-FRET) fluorescence assay was developed to directly monitor dimerization of PKR kinase domains induced by RNA binding. Homo-FRET occurs between fluorophores of the same kind provided the Stokes shift is small, and is readily detected by depolarization of the emission using steady-state anisotropy measurements. Based on the dsRNA dissociation constants for PKR[59], the equilibrium populations of PKR dimers are expected to be low and we have used homo-FRET to assay PKR kinase domain dimerization due to the high precision of the measurement and convenience of labeling. Because PKR contains 8 cysteines, 7 of which are highly conserved, unnatural amino acid mutagenesis[67] was employed to introduce a single *p*-azido phenylalanine (*p*AzF) residue into wild-type PKR for labeling

with extrinsic fluorophores (Fig. 4.2.A.). Labeling sites were selected based on their proximity, solvent accessibility, and lack of interference with the dimer interface. Highly conserved residues were excluded. The K261*p*AzF mutant was chosen for detailed analysis based on high expression, ease of labeling, and efficient homo-FRET.

K261*p*AzF PKR reacts readily with Alexa Fluor 488-dibenzocyclooctyne to produce a stable conjugate, denoted *p*AzF-261-A488. The integrity of the labeled protein was monitored by autophosphorylation assays, dsRNA binding, and solution dimerization analysis. *p*AzF-261-A488 is an active kinase and undergoes autophosphorylation upon addition of a 40 bp dsRNA at a level about 2.5 -fold higher than unlabeled PKR (Fig. 4.1.A). As previously observed for unlabeled PKR[13,59], two monomers of *p*AzF261-A488 bind to the activating 40 bp dsRNA with comparable dissociation constants (Fig. 4.1.B). As assayed by sedimentation equilibrium experiments in the absence of RNA, pAzF261-A488 PKR undergoes reversible dimerization with K_d = 94 (85, 103) μM (Figure 4.1.C) which is ~5 fold lower than the K_d for dimerization of unlabeled PKR[31]. The enhancement in activation of *p*AzF-261-A488 relative to unlabeled PKR may be due to the tighter dimerization. This enhancement in dimerization is not observed for PKR labeled at position 371, which is more distant from the dimer interface (K_d = 1,260 μM). However, the energy transfer efficiency is too low for useful analysis. For the *p*Az-F261-A488 dimer, the predicted inter-chromophore distance is R = 25 Å (Figure 4.2.B) and R_0 for Alexa Fluor 488 is 48 Å[39], with a corresponding energy transfer efficiency is 98% and a steady-state anisotropy about half the monomer value.

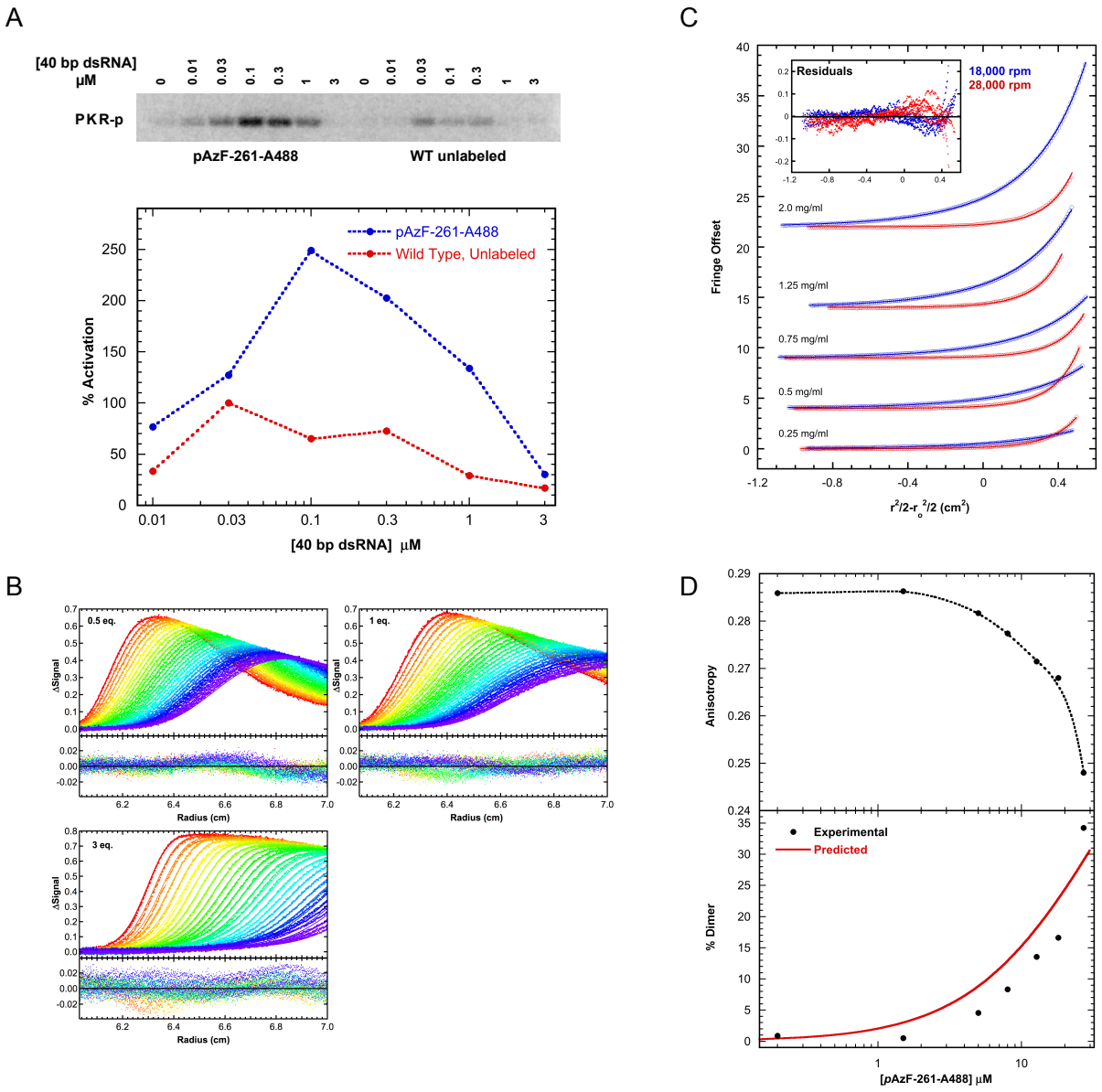

Figure 4.1.: Characterization of *p*AzF-261-A488. (*A*) Activation of *p*AzF-261-A488 by 40 bp dsRNA. Top: Phosphorimager analysis of unlabeled PKR (red) and *p*AzF-261-A488 (blue) activation. Bottom: quantitation. Data were normalized to unlabeled PKR at 30 nM 40 bp. (*B*) Sedimentation velocity analysis of *p*AzF-261-A488 binding to 0.75 μM 40 bp dsRNA. Global analysis of difference curves for at three concentrations of *p*AzF-261-A488 fit to a 2:1 binding model provides best-fit dissociation constants of K_{d1}=

0.324 (0.280, 0.376) μM and K_{d2} = 0.517 (0.448, 0.579) μM with RMSD = 0.0060 OD. The top panels contain the data (points) and fits (lines) and the bottom panels contain the residuals. (*C*) Sedimentation equilibrium analysis of *p*AzF-261-A488 self-association. Global analysis of 5 concentrations and two rotor speeds (18000 rpm – blue, 28000 rpm – red) to a monomer-dimer model results in K_d = 94 (85, 103) μM with RMSD = 0.0327 fringes. (*D*) Fluorescence anisotropy analysis of *p*AzF-261-A488 dimerization in the absence of dsRNA. Top: raw anisotropy as a function of concentration. Bottom: experimental % dimer calculated from the anisotropy data compared to the % dimer predicted using the K_d determined by sedimentation equilibrium of 94 μM. The slits were adjusted during the titration to maintain the count rate in the linear range.

4.2.2. PKR Dimerization by duplex RNAs

Significant anisotropy changes are induced by binding of *p*Az-F261-A488 to duplex RNAs (Fig. 4.2.C). The anisotropy decreases upon addition of dsRNAs ≥ 30 bp capable of activating PKR and binding two or more monomers, but non-activating, 20 and 25 bp duplexes that bind a single PKR produce negligible anisotropy changes[60]. Thus, RNA binding alone does not significantly affect the steady state anisotropy of *p*AzF261-A488,

and the depolarization induced upon addition of the longer duplexes can be ascribed to homo-FRET within kinase domain dimers. Note that the dsRBD is separated from the kinase domain by a long (~ 90 residue) unstructured linker, so that the changes in rotational correlation time of the dsRBD due to RNA binding are not expected to affect the kinase.

Quantitative analysis of the anisotropy changes produced by the activating dsRNAs provides useful mechanistic insights. The amplitude of the anisotropy change increases with the length of the dsRNA, but even for the longest (40 bp) RNA the maximum decrease of 12% does not approach the ~50% effect predicted by theory. Also, the anisotropy returns to the monomer value at higher RNA concentrations. This behavior is consistent with a simulation of the sequential binding equilibria for *p*AzF261-A488 interacting with the 40 bp RNA (Fig. 4.2.D). RNA-induced formation of the kinase domain dimer requires that two PKR monomers bind to the same RNA. The maximum population of the species containing two bound PKRs, denoted RP_2, corresponds to 14% of the total PKR (Table 4.1.) and decreases at higher dsRNA concentration due to dilution of PKR monomers onto separate strands. The amplitude of anisotropy changes for the 40 bp dsRNA indicates that a maximum of ~30% of the kinase domains exist as dimers (Table 1). If the kinase domains quantitatively formed dimers upon sequential binding of two PKR monomers to an RNA, the ratio of % dimer to % RP_2 would equal one. For the 40 bp dsRNA this value is about two, implying that the maximum dimer population must be overestimated due to additional sources of depolarization, such as a small population of RNAs containing three bound PKRs. Regardless of the origin of this discrepancy, the shape of the anisotropy titration is consistent with the RNA

concentration dependence of the RP_2 species and the amplitude implies that RNA-induced dimerization of the kinase domain occurs efficiently upon sequential binding of two PKR to the same RNA.

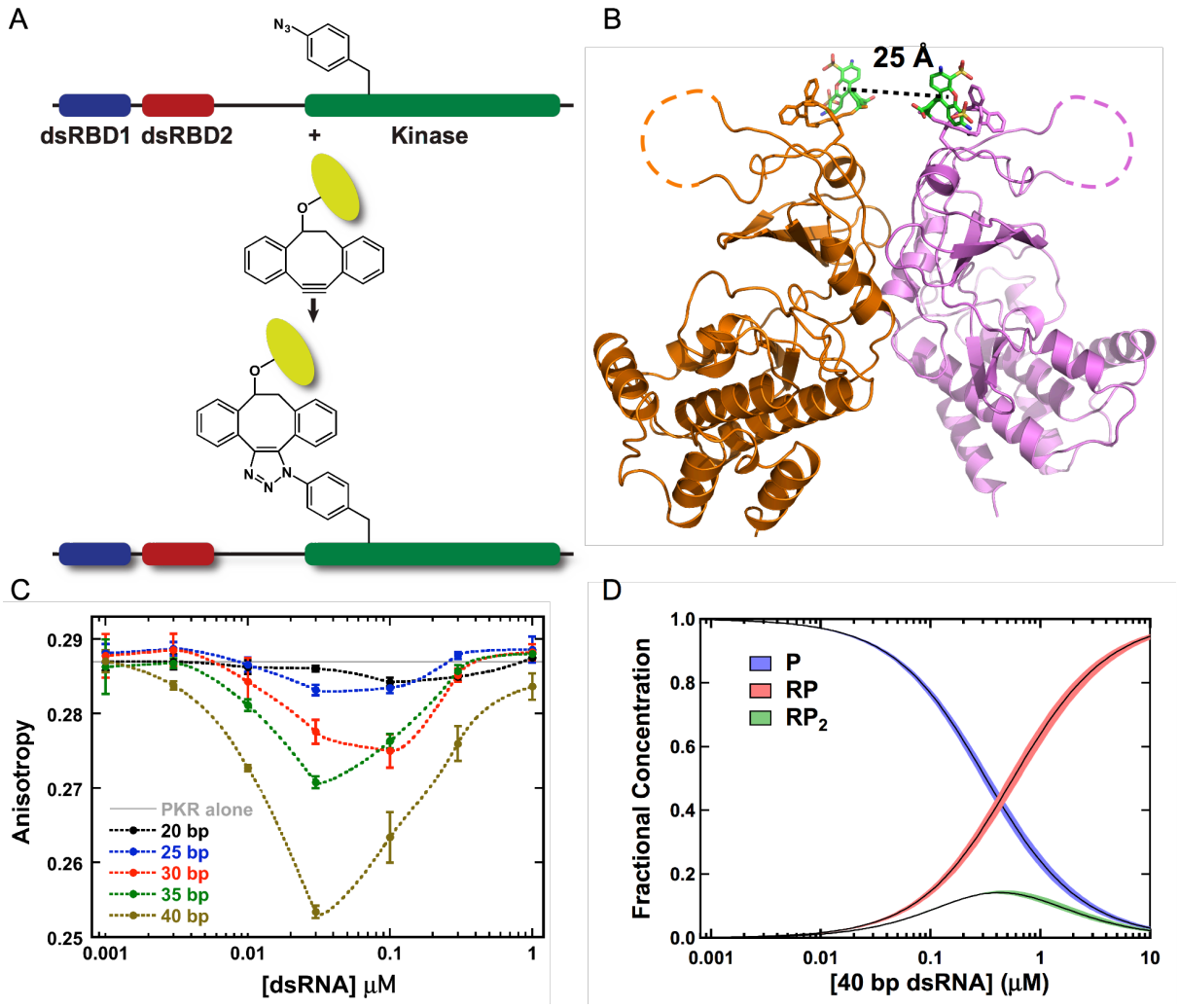

Figure 4.2. Analysis of PKR dimerization induced by activating dsRNAs. (*A*) Conjugation of fluorophores with *p*AzF-substituted PKR. (*B*) Structure of the PKR kinase domain parallel dimer (PDB accession 2A1A) rendered in PyMol (Schrödinger). Alexa Fluor 488 DIBO conjugated at *p*AzF-261 was modeling onto the structure, with the ligand indicated in stick representation and the chromophore in green. (*C*) Anisotropy

titrations of *p*AzF-261-A488 with dsRNAs. Samples contained 200 nM *p*AzF-261-A488. (*D*) Species distribution for *p*Az-F261-A488 binding to the 40 bp dsRNA. The fractional concencentrations of free protein (P, blue), the the 1:1 complex (RP, red) and the 1:2 complex (RP_2, green) are plotted. The fractional concentrations were determined using the experimentally determined dissociation constants K_{d1}= 0.324 μM and K_{d2} = 0.517 μM (Fig. 4.1). The width of the distributions correponds to the one standard deviation confidence intervals.

Control experiments confirm that the dsRNA-induced anisotropy changes are due to FRET within kinase domain dimers. The fluorescence anisotropy of pAz-F261-A488 in the absence of RNA decreases at high protein concentrations consistent with formation of a dimer (Fig. 4.1.D). The extent of dimerization is on the order predicted by the K_d measured by sedimentation equilibrium. Addition of unlabeled PKR to *p*AzF-261-A488 is expected to reduce the extent of homo-FRET by formation of mixed labeled/unlabeled heterodimers. Assuming random formation of heterodimers, the anisotropy change should be linearly in the fraction of labeled PKR. For higher oligomers a nonlinear dependence is predicted. Figure 4.3.A demonstrates that mixing increasing amounts of unlabeled PKR with *p*AzF-261-A488 linearly reduces the anisotropy decrease induced by binding to a 40 bp dsRNA (R = 0.991 for a linear fit). Alexa Fluor 488 can serve as an efficient FRET donor to Cy3 (R_0 ~ 67 Å). The fluorescence spectrum of a 1:1 mixture of PKR labeled at *p*AzF261 with Alexa Fluor 488 and Cy3 overlays with the sum of the spectra of the two components, indicating the absence of FRET (Fig. 4.3.B). Binding of

the mixture to the 40 bp dsRNA results in significant donor quenching and enhanced Cy3 emission due to hetero-FRET. These data support the model where binding of two PKRs to an activating RNA induces formation of kinase domain dimers.

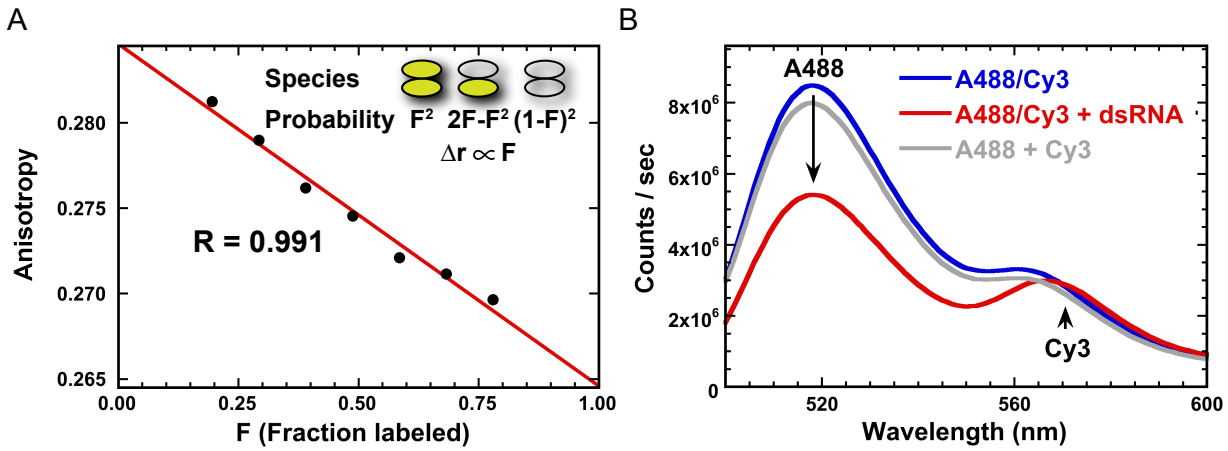

Figure 4.3. Depolarization is due to FRET-induced dimerization. (*A*) Dependence of anisotropy on the fraction of labeled PKR. Samples contained 100 nM 40 bp dsRNA and 200 nM *p*Az-F261-A488. (*B*) Analysis of PKR dimerization by hetero-FRET. Donor: *p*Az-F261-A488, acceptor: *p*Az-F261 PKR labeled with DIBO-Cy3. Spectra: 1:1 mixture (200 nM total) of donor and acceptor (blue), 1:1 mixture (200 nM total) of donor and acceptor with 100 nM 40 bp dsRNA (red), algebraic sum of 100 nM donor and 100 nM acceptor spectra (grey).

4.2.3. PKR dimerization with catalytically inactive constructs

In the PKR dimer interface, R262 forms a salt bridge with D266 (Fig. 3A) and disruption of this interaction in a R262D PKR mutant blocks kinase activity[44]. Similarly, disruption of a hydrogen-bonding interaction between Y323 and D289 in PKR Y323A reduces activation. We expected that these mutations block PKR activation by preventing kinase dimerization and would serve as negative controls for the homo-FRET assay. Surprisingly, fluorescence anisotropy titrations indicate that *p*AzF-261-A488 containing either interface mutation undergoes dimerization upon binding to the 40 bp dsRNA (Fig. 4.4.B). The maximal amplitudes of the anisotropy changes are somewhat smaller than observed for wild-type PKR with a corresponding Dimer/RP_2 ~ 0.8 (Table 4.1.). PKR autophosphorylation assays confirm that these constructs are inactive (Fig. S2). Consistent with the anisotropy data, sedimentation equilibrium analysis of R262D PKR demonstrates reversible dimerization in free solution with K_d of 923 (714, 1267) μM (Figure 4.4.C), or about 2-fold weaker than WT. Similarly, Y323A PKR also dimerizes with a K_d of 689 (590, 820) μM. Thus, the disruption of interdimer salt-bridge or hydrogen bonding interactions abolishes PKR activation while only slightly reducing dimerization affinity.

The reduction in the Dimer/RP_2 ratio for R262D indicate less efficient dimerization or the dimers may have an altered geometry that induces less depolarization. Formation of an antiparallel dimer modeled on the GCN2 structure would increase the distance between *p*AzF-261-A488 fluorophores from 25 to 49 Å resulting in diminished energy transfer. To test this model, wild-type and R262D PKR were labeled position 301 where the energy transfer efficiency should be enhanced in a GCN2-type antiparallel, inactive

dimer relative to the active parallel structure, with interfluorophore distances of 24 and 60 Å, respectively. Titration of either *p*AzF-301-A488 or *p*AzF-301-A488/R262D PKR with 40 bp dsRNA results in a similar low amplitude anisotropy change indicating that the inactive R262D dimers likely do not adopt a GCN2-type structure.

The 20 bp dsRNA binds a second PKR upon reducing the concentration of NaCl from 200 to 75 mM[13,59]. Although this short RNA does not activate PKR at either NaCl concentration[59], it does induce an anisotropy change in 75 mM NaCl (Fig. 4.4.D) corresponding to a maximum dimer population of about 9%. However, PKR binds very strongly to the 20 bp RNA at low salt so that the maximum population of RP_2 is high (49%), resulting in Dimer/RP_2 of only 0.19 (Table 4.1.). Thus, only a small fraction of the bound PKRs form dimers upon binding to this short dsRNA.

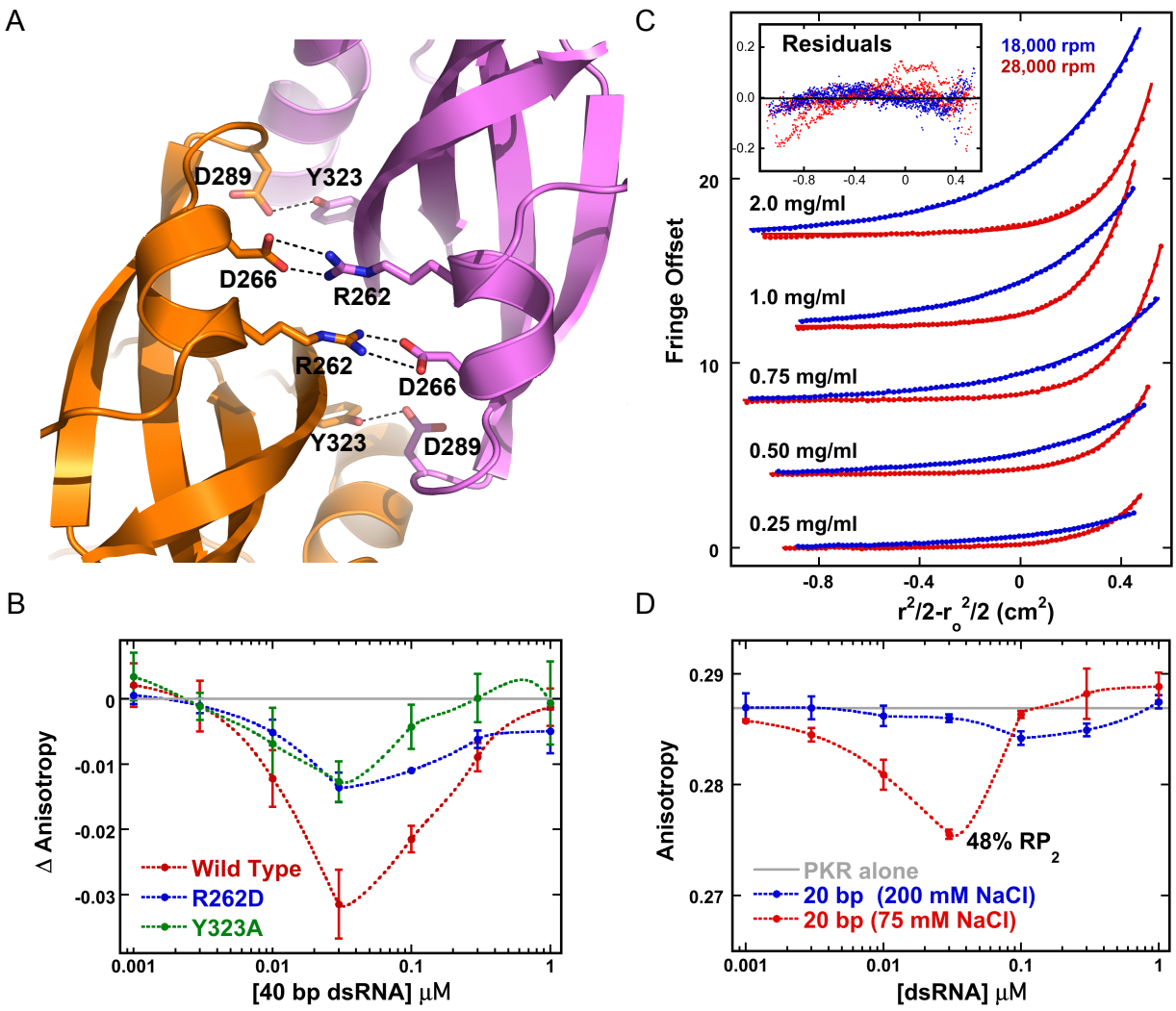

Figure 4.4. Dimerization without activation of PKR. (*A*) Critical intermolecular salt bridge (R262 – D266) and hydrogen bond (Y323-D289) interactions in the PKR kinase dimer interface (PDB accession 2A1A) rendered in PyMol (Schrödinger). (*B*) Anisotropy titration of *p*AzF-261-A488 (red), pAzF-261-A488-R262D (blue) and pAzF-261-A488-Y323A (green) PKR with 40 bp dsRNA. The anisotropy of the free protein was subtracted from each data set. (*C*) Sedimentation equilibrium analysis of R262D PKR. The points are the data and the solid lines are the best fit. For clarity, only every fourth point is shown. The inset shows the residuals. Global analysis reveals that R262D

dimerizes, with a best-fit K_d = 923 (714, 1267) μM (the values in parentheses correspond to the one standard deviation confidence intervals) and an RMS deviation of 0.041 fringes. The K_d for WT PKR dimerization under the same conditions is 450 μM. (*D*) Anisotropy titration of pAzF-261-A488 PKR with a 20 bp dsRNA in AU200 and AU75 buffer.

4.2.4. Dimerization on barrier containing RNAs

Introducing of helical imperfections into dsRNAs typically reduces PKR binding and to activation[68,69]. However, PKR is also activated by certain RNAs that contain bulges, loops, pseudoknots and single-stranded tails[42]. PKR can be activated by dimers of TAR[30] and the HDV ribozyme[70] that contain short duplex regions separated by a distorted central region that serves as a barrier. To systematically probe the effect of structural distortions on PKR dimerization and activation by dsRNA, we introduced structurally defined, inert, rigid barriers into a model duplex. The dsRBD interacts with the RNA 2'-OH[52] and the barriers consist of 2'-O-methyl dsRNA. The RNAs contain two 15 bp dsRNA regions, the minimal length required to each bind one PKR with high affinity, separated by variable length 2'-O-methyl dsRNA barriers and are denoted as X-Me, where X is the length of 2'-O-methyl dsRNA (Fig. 4.6.A). PKR is not activated by 2'-O-methyl dsRNA[71] and does not bind to a 15 bp 2'-O-methyl duplex RNA (Fig. 4.5.).

PKR binding to the barrier-containing RNAs was characterized using sedimentation velocity analytical ultracentrifugation. As expected, each of the RNAs binds two PKR monomers (Table 2). The dissociation constants for 5-Me are similar to a 30 bp dsRNA

(zero-length barrier)[13]. The dissociation constants for the binding of the first PKR are not very sensitive to barrier length but K_{d2} increases systematically from 5-Me to 15-Me.

PKR activation was strongly affected by the introduction of longer barriers (Fig. 4B). 5-Me activated PKR but 10-Me and 15-Me elicited little to no autophosphorylation. These results are supported by previous work where introduction of a 11 bp DNA-RNA chimeric duplex between two 20 bp dsRNAs greatly attenuated PKR activation[68]. Binding of *p*AzF261-A488 to all three barrier-containing dsRNAs results in a significant anisotropy decrease due to kinase domain dimerization (Fig. 4C). The maximal anisotropy change is slightly attenuated with increasing barrier length, but even for the inactive 10-Me and 15-Me constructs it is comparable to that induced by the activating 30 bp dsRNA. All three RNAs have a high Dimer/RP_2, indicating efficient kinase domain dimerization.

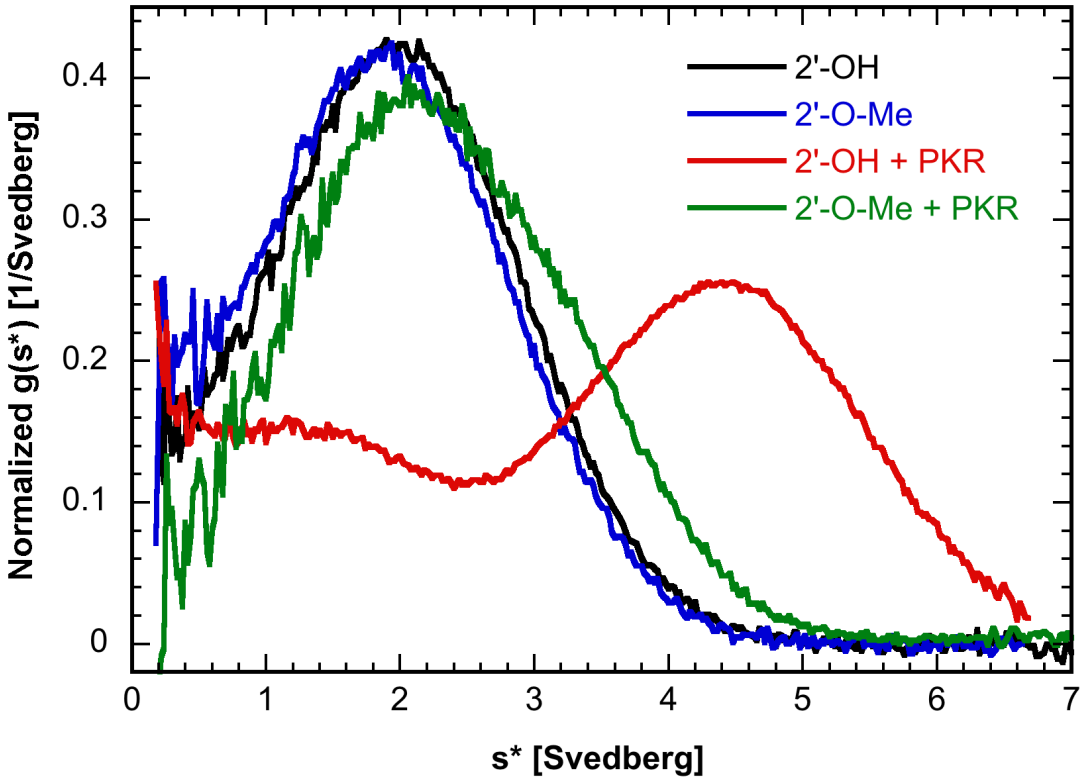

Figure 4.5: Sedimentation velocity analysis of PKR binding to 2'-OH and 2'-O-Me dsRNAs. Normalized *g(s*)* distributions of 2.3 μM 15 bp 2'-OH dsRNA (black), 2.3 μM 15 bp 2'-O-Me dsRNA (blue) 2'-OH dsRNA + 2 eq. PKR (red), 2'-O-Me dsRNA + 2 eq. PKR (green). The peak of the distribution for the 2'-OH dsRNA shifts to a higher sedimentation coefficient in the presence of PKR due to the formation of a 1:1 complex. A similar shift is absent for the 2'-O-Me dsRNA, indicating that PKR does not bind. The shoulder present in the 2'-O-Me dsRNA + PKR sample is due to a contribution from free PKR (s ~ 3.5 S).

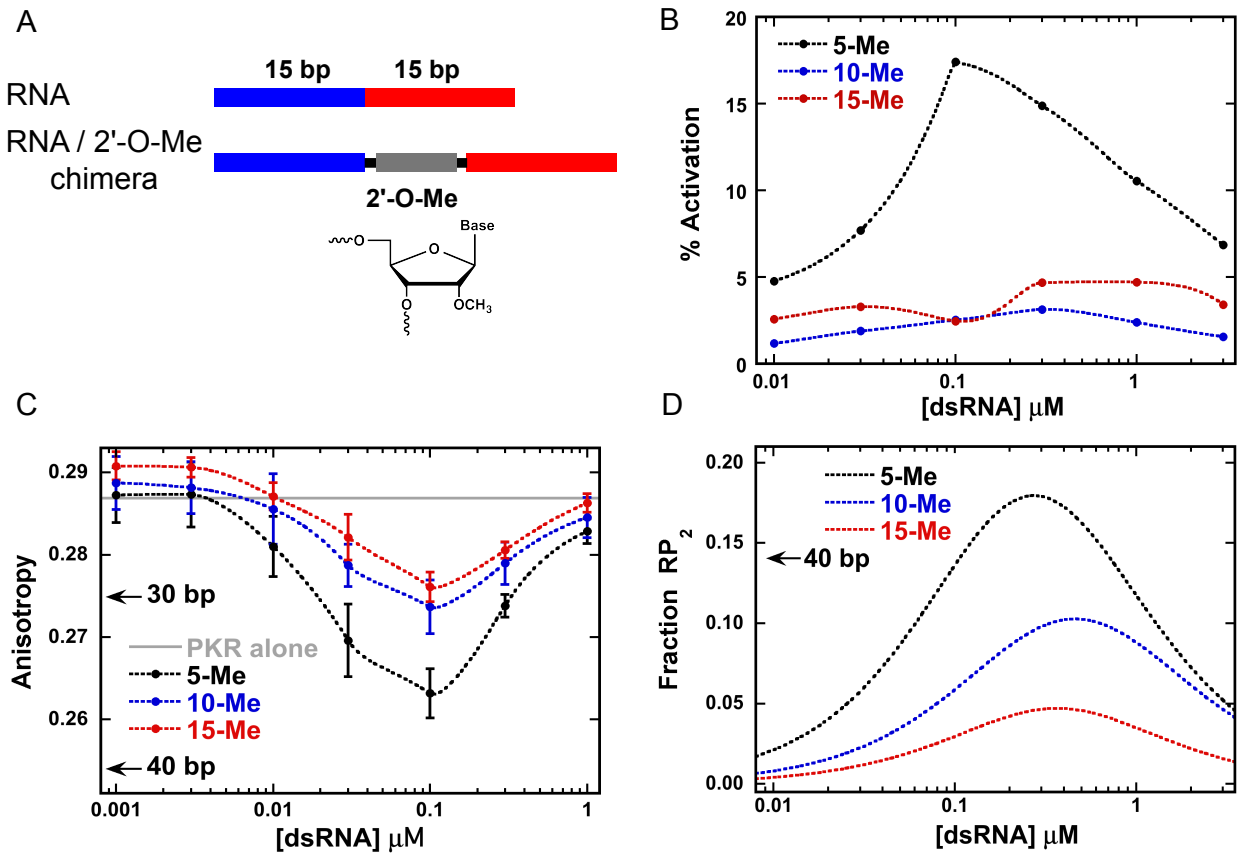

Figure 4.6 Interaction of PKR with dsRNAs containing 2'-O-methyl barriers. (*A*) Schematic of 2'-O-methyl (2'-O-Me) barrier-containing dsRNAs. Chimeric dsRNAs were designed to contain 5, 10 and 15 bp 2'-O-Me barriers inserted between two 15 bp dsRNA regions. (*B*) Activation of WT PKR by 2'-O-Me barrier-containing dsRNAs. The percent activation is normalized to signal from the 40 bp dsRNA at 100 nM. (*C*) Anisotropy titration of pAzF-261-A488 PKR with 2'-O-Me barrier-containing dsRNAs. For reference, the maximal anisotropy changes associated with PKR binding to regular 30 and 40 bp dsRNAs are indicated by arrows. (D) Fractional concentrations of the 1:2 RNA:PKR complex (RP_2) for PKR binding to the 2'-O-Me barrier-containing dsRNAs. The fractional concentrations were determined using the experimentally determined

dissociation constants (Table 4.1.). The maximal fraction of RP_2 for PKR binding to a 40 bp dsRNA is indicated with an arrow.

Table 4.1. Correlation of PKR dimerization and RNA binding.

Sample	Max. % Dimer[a]	Max. % RP_2[b]	Dimer / RP_2[c]
WT + 40 bp	29.5 ± 0.6	14.3 ± 1.4[d]	2.06 ± 0.21
R262D + 40 bp	11.4 ± 1.5	14.3 ± 1.4[d]	0.80 ± 0.13
Y323A + 40 bp	11.1 ± 2.2	14.3 ± 1.4[d]	0.77 ± 0.17
WT + 20 bp (75 mM NaCl)	9.2 ± 0.3	48.8 ± 3.7[e]	0.19 ± 0.02
WT + 5-Me	20.9 ± 2.1	18.0 ± 1.6[f]	1.16 ± 0.16
WT + 10-Me	11.6 ± 2.3	10.3 ± 1.8[f]	1.13 ± 0.30
WT + 15-Me	9.5 ± 1.3	4.7 ± 0.4[f]	2.02 ± 0.32
WT + HO-ss-dsRNA	24.2 ± 0.5	15.0 ± 1.2[g]	1.61 ± 0.13
WT + ppp-ss-dsRNA	24.6 ± 0.5	21.1 ± 1.8[g]	1.16 ± 0.10

[a]Maximum % dimer calculated from the largest anisotropy change and the anisotropy of the dimer

[b]Maximum population of RP_2 species based on K_{d1} and K_{d2} for sequential binding of two PKR monomers under the conditions indicated.

[c]The ratio of the maximal % dimer to the maximal % RP_2.

[d]Data from Fig. 1.

[e]Previously reported[13]

[f]Data from Table 4.2.

[g]Mayo C., Wong, C.J. and Cole, J.L. (Submitted).

Table 4.2. Analysis of PKR binding to barrier-containing dsRNAs.

RNA	K_{d1} (nM)	K_{d2} (nM)	RMS[b]
5-Me	173 (127, 235)	375 (319, 440)	0.0067
10-Me	360 (263, 492)	784 (606, 1036)	0.0082
15-Me	266 (231, 306)	1,930 (1709, 2194)	0.0091

Parameters were obtained by global nonlinear least square analysis of sedimentation velocity measurements. The values in parentheses represent the 95% joint confidence intervals obtained using the F-statistic.

[a]Uncorrected sedimentation coefficient (Svedbergs).

[b]Root mean square deviation of the fit in absorbance units.

Discussion

The homo-FRET assay directly probes PKR kinase domain dimerization on RNA and provides new insights into the factors that distinguish RNA activators and inhibitors. As previously inferred[43], dsRNA activators promote kinase domain dimerization and the extent of dimerization correlates with activation potency. These data support a dimerization model[43,45] where activating duplex RNAs function to bring PKR monomers into close proximity, leading to dimerization of the kinase domains.

PKR binds to dsRNA nonspecifically in multiple configurations[20] so that PKR monomers may be quite far apart along the nucleic acid lattice. Thus, it is noteworthy that duplex RNA activators ≥30 bp induce efficient dimerization following assembly of two PKRs onto a single RNA. Other proteins harboring dsRBDs can travel along

dsRNA by passive diffusion[72] and efficient assembly of kinase domain dimers may occur via this mechanism.

In contrast to longer dsRNAs, kinase domain dimerization is inefficient on short, nonactivating dsRNA that bind two PKRs in low salt. The impaired dimerization for short duplexes is correlated with a difference in RNA binding mode. Affinity cleavage[51], NMR shift perturbation[20] and RNA binding analyses[20,59] reveal that short dsRNAs that fail to activate predominantly interact with dsRBD1 whereas longer activators interact extensively with both dsRBDs. Thus, interaction of dsRBD2 with RNA appears to regulate kinase domain dimerization despite that fact that these regions are separated by a long linker. Although this linker is unstructured in the free enzyme[34,35,56], it may become at least partially ordered in the presence of RNA and serve to sterically regulate kinase domain interactions.

In contrast to perfect duplexes, the correlation between PKR activation and kinase domain dimerization breaks down in the context of more complex RNAs, indicating that dimerization is required but not sufficient to activate the kinase. Abrogation of PKR activation by insertion of 2'-O-Me dsRNA barriers ≥ 10 bp does not appreciably affect the efficiency of dimerization. A barrier of 10 bp of A-form RNA duplex corresponds to a distance along the helical axis of only ~ 28 Å. It is reasonable that the barrier does not disrupt dimerization given that the linker between the dsRBD and the kinase is long and would be capable of spanning this short distance. However, the larger barriers induce a change in RNA binding mode that modulates activation, indicating long-range communication between the dsRBDs and kinase domain. The structural basis for the dramatic dependence of activation on barrier length is not clear. The effect of barrier

length on binding affinity for the second PKR (Table 4.1.) implies that weak cooperative interactions that stabilize binding of the second PKR become attenuated as the length of the barrier increases.

The relationship between PKR dimerization and activation can be interpreted within the broader context of the other members of the eIF2α family of protein kinases. PKR[17,73] and PERK[63] share a similar back-to-back parallel parallel dimer and conservation of interface residues suggests that this structure is a common element among the other eIF2α kinases. We propose that PKR activation requires formation of a back-to-back parallel interface. Although R262D and Y323A PKR mutations that disrupt interdimer salt bridge and hydrogen-bonding interactions block PKR activation[44,66] (Fig. 4.4) they do not prevent dimerization at high concentration in the absence of RNA or upon binding to an activating dsRNA. Although the energy transfer efficiency of *p*AzF-261-A488 is reduced by these mutations, implying a rearragement in the dimer interface, it is not enhanced in *p*AzF-301-A488/R262D, indicating that the inactive dimer does not correspond to the model based on the antiparallel GCN2 interface. Some nonactivating RNAs, such as the 20 bp duplex, bind multiple PKRs but fail to induce kinase domain dimerization. Other nonactivating RNAs, such as the barrier containing molecules, induce formation of an inactive dimer configuration analgous to that found in the R262D and Y323A PKR mutants. The allosteric pathway linking the PKR dimer interface to the kinase active site is likely disrupted in this configuration[17,57].

The inactive PKR dimer configuration may provide an additional mechanism for distinguishing between host and pathogen RNA. High throughput transcriptional analysis has revealed the presence of hundreds of dsRNAs in human cells[74]. PKR must

be able to distinguish host RNAs from pathogen-derived molecules to avoid inappropriate activation of the innate immunity response. One level of recognition is achieved based on dsRNA length, where a minimum of ~30 bp of duplex are required for activation[12,13,19,59]. Here, regulation of PKR is controlled by dimerization; short duplexes do not induce dimerization (Fig. 4.4D). In other cases, regulation may be controlled by the dimer orientation. Our analysis of 2'-O-methyl barrier-containing duplexes suggests that some secondary structure defects may regulate PKR activation by induction of inactive dimers and this may serve to prevent aberrant response to host transcripts.

Chapter 5: Role of the inter-domain linker

5.1. Introduction

PKR is comprised of two N-terminal dsRNA binding domains (dsRBD) and a C-terminal kinase domain (Fig. 1a). The dsRBDs are separated by a short (~20 amino acid) linker. NMR analysis indicates that this linker is disordered[18]. In the human enzyme, the regulatory and catalytic domains of the protein are separated by a long, ~90 amino acid linker. Residues 169-229 at the N-terminal end of the linker have the signatures of an intrinsically disordered region (Fig. 1b) with low sequence complexity and high content of uncharged polar side chains. The C-terminal portion (229-258) is enriched in basic residues. AFM[56], NMR[35] and SAXS[34] indicate that the linker is flexible and PKR can adopt a range of closed and open conformations. The PKR kinase domain crystalizes as a dimer[17,73] and biochemical and biophysical analyses support a pivotal role for dimerization in activation[43]. PKR dimerizes only weakly (K_d ~ 500 μM); however, this reaction induces autophosphorylation in the absence of dsRNA[31]. The isolated kinase domain is not autoactivated; however, constructs including the adjoining basic region (228-551) or the entire linker (169-551) are activated in the absence of dsRNA, implying that the basic domain may contribute to dimerization or regulate activation.

The role of the long interdomain linker in PKR is not well understood. There is evidence of long-range communication between the dsRBDs and kinase domain. Kinase domain dimerization is inefficient on short, nonactivating dsRNA that bind two PKRs in low salt (Husain, B., Hesler S. and Cole, J.L., submitted), suggesting that the dsRNA binding mode affects kinase dimerization. Insertion of 2'-O-Me inert dsRNA

barriers in the middle of a 30 bp dsRNA blocks PKR activation but does not impede dimerization (Husain, B., Hesler S. and Cole, J.L., submitted). Thus, dimerization is required but not sufficient to activate the kinase and these barrier-containing RNAs induce a nonproductive kinase dimer configuration. Although the long linker is predominantly unstructured in the free enzyme it may become ordered upon binding RNA. Interestingly, the sequence and length of the N-terminal portion of the linker are not conserved among mammalian PKR sequences and it is virtually absent in the Syrian golden hamster (*M. auratus*) (Fig. 1b). This natural variability suggests that this region does not play a critical role in the activation mechanism. However, the contribution of the linker to the structure and function of PKR has not been assessed. Here, we characterize the functional properties and conformation of a human PKR construct lacking the variable region that is analogous to the *M. auratus* enzyme. Removal of the variable linker results in quantitative but not qualitative changes in activation, dsRNA binding and flexibility.

5.2. Results

5.2.1. Rationale for studying hamster PKR ortholog

In order to explore the importance of the variable region of the linker, we set out to characterize hamster (*M. auratus*) PKR, a naturally occurring PKR variant in which this region is largely absent. Outside of the linker region missing in the hamster enzyme, human and hamster PKR are very closely related, with about 60% sequence identity. Hamster PKR is does not yield soluble protein when it is expressed in *E. coli* using conditions optimized for the human enzyme[31]. Expression at lower temperature in Arctic

Express RIL DE3 cells that supply cold shock chaperones results in increased solubility. However, the Cpn-10 chaperone binds strongly to hamster PKR and it was not feasible to produce large amounts of pure enzyme. Sedimentation velocity measurements indicate that hamster PKR binds to a 40 bp dsRNA(Fig. 5.1.A). The g(s*) distributions shift to the right with increasing protein concentration. The magnitude of the shift indicates that three PKRs bind to the 40 bp RNA. In contrast only two human PKR bind to this RNA under identical condition[13,59]. Hamster PKR is activated by 40 bp dsRNA in a bell-shaped manner analogous to human PKR (Fig 5.1.B). However, the maximum extent of phosphorylation is ~8 fold higher for the hamster enzyme. The increased activation potency may be associated with the higher binding stoichiometry.

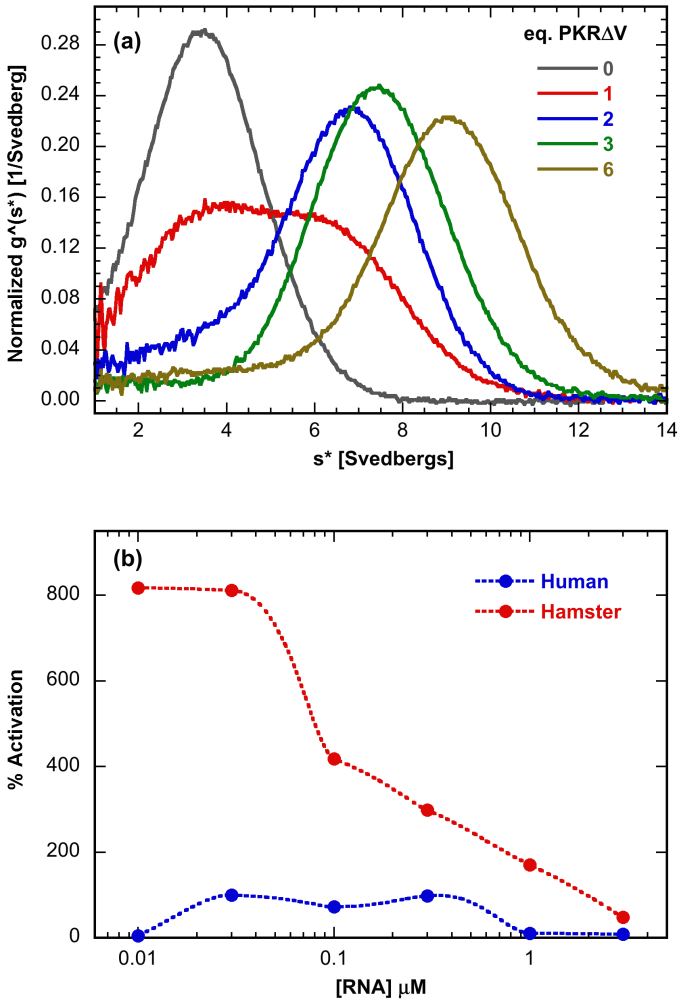

Figure 5.1. Functional characterization of Hamster PKR. (a) g(s*) analysis of 40 bp and Hamster PKR. 0.75 μM 40 bp dsRNA was mixed with 1-6 equivalents of Hamster PKR and the rate of sedimentation was measured by absorbance AUC. The shift of the peak of the g(s*) distributions to ~ 9S at 6 equivalents corresponds to a 3:1 PKR:dsRNA complex. b) Hamster PKR activation by 40 bp dsRNA. Activation was measured with various concentrations of dsRNA and 100 nM of hamster (red) and human (blue) PKR at 32^{o}C for 15 minutes with 4 μCi of ATP γ-^{32}P and 0.4 mM ATP. The samples were

analyzed by SDS PAGE analysis and autoradiography. Hamster PKR is activated ~8 fold more potently than human PKR.

5.2.2. Functional characterization of PKRΔV

Due to the practical limitations of obtaining pure hamster PKR we examined an analogous construct derived from human PKR in which the variable region (170-228) is deleted. This construct, denoted PKRΔV (Fig. 5.2.A), displayed an appreciable improvement in solubility and stability relative to hamster PKR. The activation and RNA binding properties of this construct are similar to the hamster enzyme (*vide infra*). A construct lacking the linker sequence, PKRΔVB was also created to probe the importance of the more conserved C-terminal basic region of the linker.

Human PKR is capable of being activated in an RNA-independent fashion at higher protein concentrations due to weak dimerization[31]. Similarly, PKRΔV also undergoes RNA-independent autophosphorylation (Fig 5.3.A). The degree of autophosphorylation increases with protein concentrations and is significantly enhanced relative to full length PKR. At lower protein concentrations where autoactivation is not present, PKR is activated by dsRNAs of 30 bp or longer. Duplex RNAs also induce PKRΔV to undergo autophosphorylation with a characteristic bell-shaped activation curve (Fig. 5.3.B). The longest dsRNA examined (40 bp) activates PKRΔV ~2.5 fold more potently than full length PKR and the maximum occurs a low dsRNA concentration of 3 nM compared to about 30 -100 nM for the full-length enzyme. The 30 bp dsRNA is a poor activator of PKRΔV and no activation is detected for the 20 bp duplex.

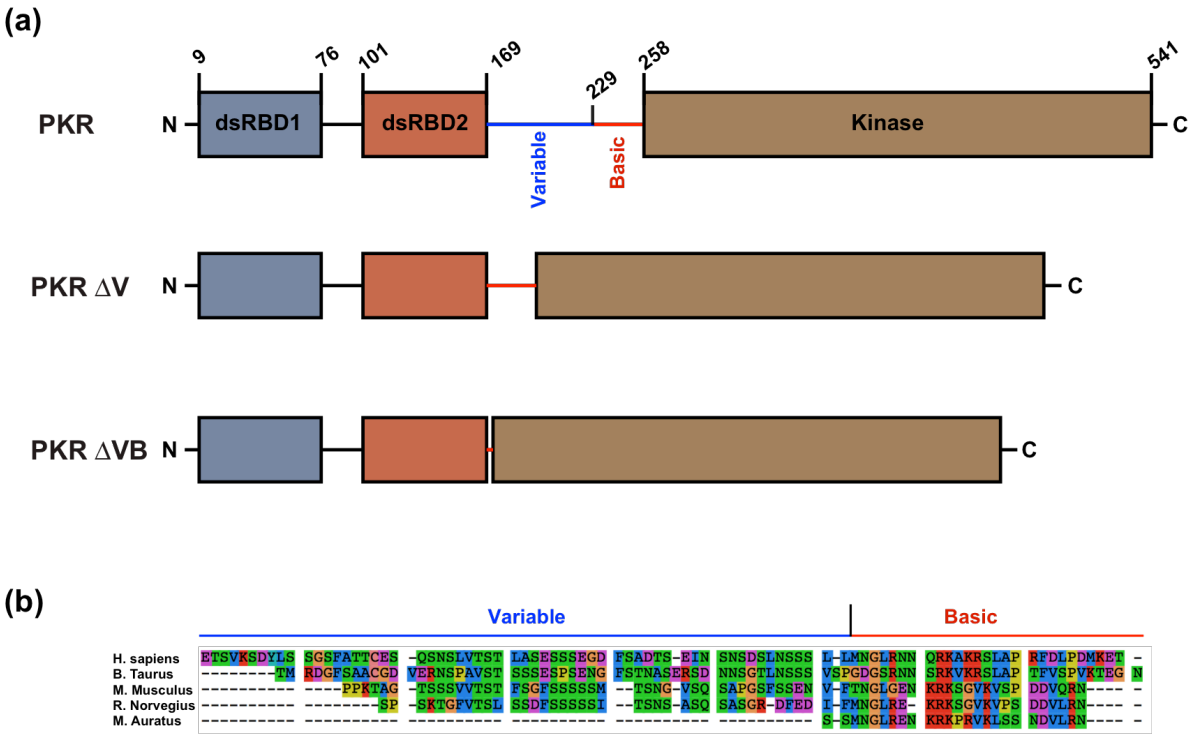

Figure 5.2. PKR domains and linker regions. (a) Domains of PKR and linker deleted constructs. The interdomain linker contains a variable region (169-229) and a basic region (229-258) depicted as blue and red solid lines respectively. The middle and bottom panels show the regions of the linker deleted and the corresponding construct nomenclature (b) Linker sequence alignment. Sequence alignment of the linker regions from various PKR homologs were aligned and illustrated using SeaView[75]. The residues are coloured based on their charge and hydrophobicity. The alignment shows the clustering of basic residues in the C terminus of the linker whereas the variable region is in fact variable in length across species.

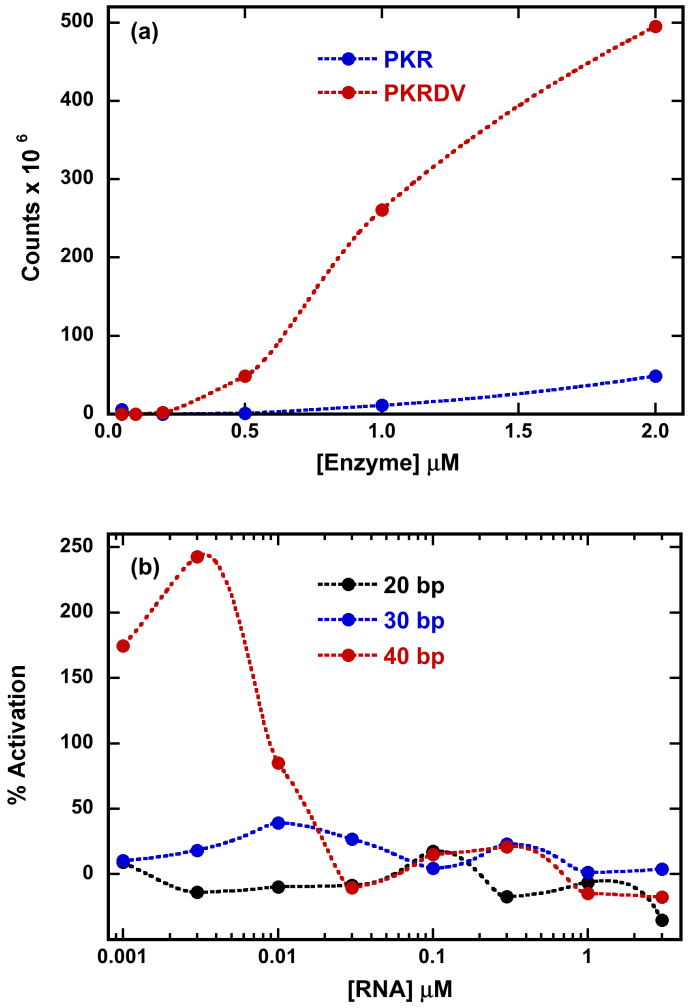

Figure 2. Effect of variable linker region on PKR activation. (a) dsRNA-independent activation**.** The extent of PKR (blue) and PKR ΔV (red) autoactivation was measured at 0.05 – 2 μM at room temperature following 10 minute incubation with 4 μCi of ATP γ-^{32}P. PKR ΔV auto-activation is ~10 fold greater than for PKR. (b) dsRNA-induced activation. PKR ΔV activation was monitored at 0.1 μM with varying concentrations of 20 bp (black), 30 (blue) and 40 bp (red) dsRNA. The percent activation is normalized against the percentage of PKR activation by 0.03 uM 40 bp dsRNA. The activation shows a bell

shaped curve and both 20 and 30 bp dsRNAs are poor activators. 40 bp dsRNA activated PKR ΔV ~2.5 times more potently than it does PKR.

5.2.2. Dimerization of PKRΔV

To test whether the increased activation of PKRΔV is due to enhanced dimerization, the dimer dissociation constant of PKRΔV was measured by sedimentation equilibrium (Fig. 5.4.). Data were collected over a protein concentration range of 0.25 - 2 mg/ml and two rotor speeds and were globally fit to a monomer-dimer equilibrium model. The best fit K_d = 1.75 (1.43, 2.21) mM, which is about three-fold weaker than for full length PKR[31]. Thus, deletion of the variable portion of the linker actually reduces the dimerization affinity, indicating that the enhanced degree of RNA-independent autophosphorylation of PKRΔV must be due to other effects.

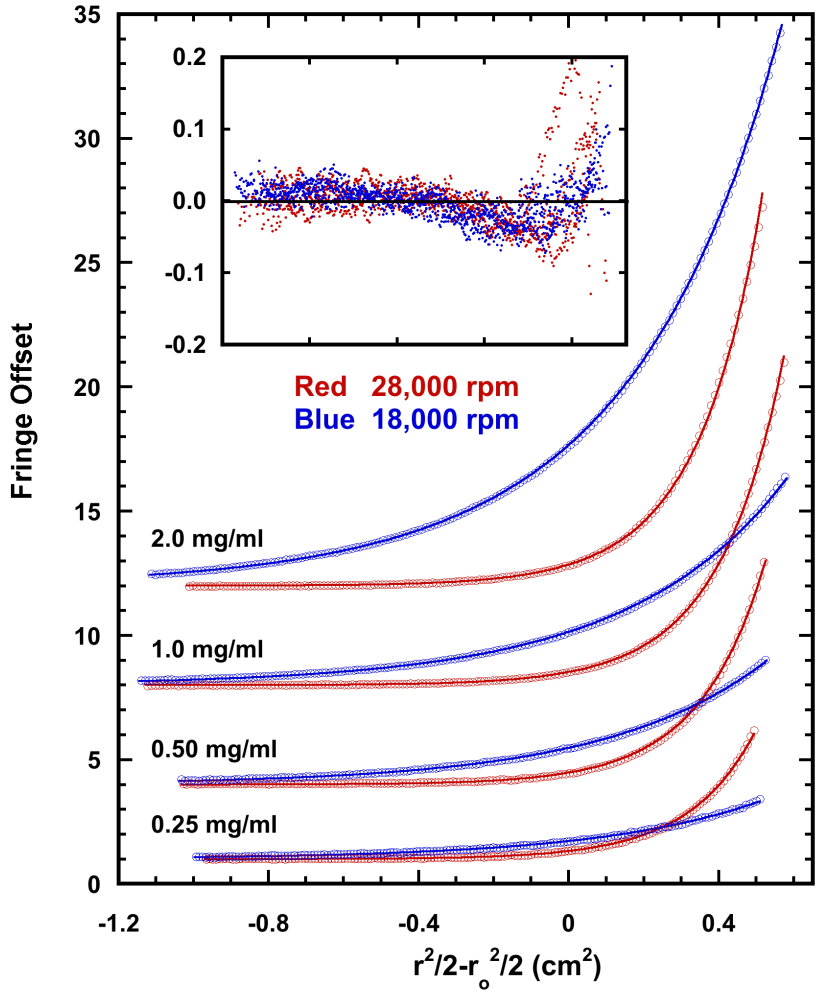

Figure 5.4. Dimerization of PKR ΔV. The Kd for self-association of PKR ΔV was measured using sedimentation equilibrium. The data (empty circles) were collected for 0.25 mg/mL, 0.5 mg/mL, 1 mg/mL and 2 mg/mL at 28000 rpm (red) and 18000 rpms (blue). The data were fit to monomer-dimer equilibrium (solid lines) using Heteroanalysis and the K_d = 1.75 (1.43, 2.21) mM. The residuals are presented in the inset as solid circles.

5.2.2. PKRΔV binding to duplex RNAs

The stoichiometries and affinities for PKRΔV binding to dsRNA were measured for 20- 40 bp sequences using sedimentation velocity and compared with full length PKR. The stoichiometries were determined from the magnitude of the shift in the g(s*) sedimentation coefficient distribution function upon titration of the dsRNA with protein[36]. For the 40 bp dsRNA, addition of 6 eq. of PKRΔV induces a large shift from ~ 3.5 S to ~ 8 S (Fig. 5.5.A), which is higher than the sedimentation coefficient for the 2:1 complex formed with full length PKR[59]. Thus, three PKRΔV bind to the 40 bp dsRNA in AU200 buffer whereas only two full-length PKR monomers bind under comparable conditions. The data obtained at four protein concentrations were globally fit to this model using SEDANAL (Fig. 5.5B). A good fit is obtained with a low RMS deviation of 0.0070 OD and small residuals. The best-fit K_ds for the first and second PKR binding events are 75 nM and 56 nM respectively with considerably weaker binding of the third monomer (Table 1). The value of K_{d1} is similar to that observed for the full length enzyme but K_{d2} is tighter[59], suggesting enhanced cooperativity of binding.

Table 1. Binding constants for PKRΔV and duplex dsRNAs

RNA	Kd_1 (nM)	Kd_2 (nM)	Kd_3 (nM)	RMSD[a]
20 bp	235 (189, 286)	-	-	0.0079
30 bp	77 (24, 215)	865 (480, 1700)	-	0.0160
40 bp	75 (43, 121)	56 (27, 99)	2,290 (1,380, 3.870)	0.0070

Parameters obtained by global nonlinear least square analysis of sedimentation velocity experiments. The values in parentheses represent the 95% joint confidence intervals obtained using the F-statistic.

[a]Root mean square deviation in absorbance units.

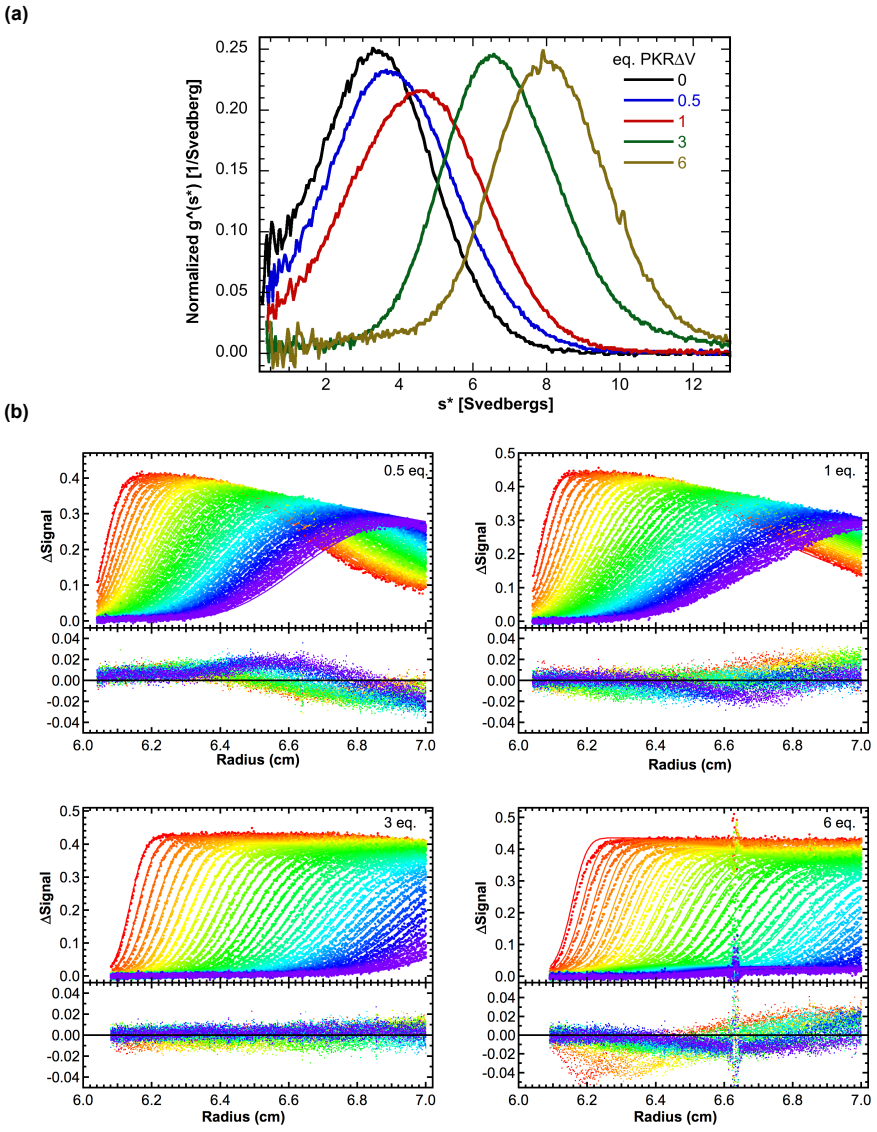

Figure 5.5. Effect of variable linker region on RNA binding. (a) g(s*) analysis. PKR ΔV binding to 40 bp dsRNA was measured using absorbance sedimentation velocity measurements. 0.75 uM 40 bp concentration was fixed and increasing equivalents of PKR ΔV were analyzed. The g(s*) analysis perfomed using DCDT+ shows that the peak of the distributions shifts to higher S indicating that protein-RNA complexes are being formed. (b) Global analysis. The data at all PKR ΔV concentrations were fit globally

using Sedfit to a 3:1 binding model. The dissociation constants and rmsds are presented in Table 1.

5.2.2. Conformation analysis of PKRΔV by small angle X ray scattering (SAXS)

Human PKR contains two flexible linker regions and adopts a range of compact and extended conformations[34]. The contribution of the variable linker region of PKR to flexibility was determined by small angle scattering analysis of PKRΔV. Data were collected over a concentration range from 1 - 5 mg/ml. The parameters derived from Guinier and GNOM analysis did not vary substantially over this concentration range so the data at the highest concentration were used for further analysis. A linear Guinier plot (Fig 5.6.A) indicates the absence of aggregation. The radius of gyration (R_g) of 33.3 Å is substantially smaller than for full length PKR (~ 40 Å)[34], indicating that PKRΔV does not adopt as extended a conformation as the wild type protein. Similar to full length PKR, the p(r) distribution of interatomic distances peaks at about 30 Å with a tail to longer distances, suggesting the presence of flexible regions. However, the D_{max} for PKRΔV is smaller (110 Å) relative to full-length PKR (175 Å). A Kratky plot of the scattering data (Fig. 5.7.) exhibits a peak at lower q and rises at higher q, which is characteristic of proteins containing both folded and disordered regions.

Based on the evidence that PKRΔV retains flexibility we have pursued structural models consisting of three folded domains (dsRBD1, dsRBD2 and kinase) connected by linkers that can adopt multiple conformations. The EOM[76,77] program was used to generate a large (10,000) pool of structures and select a minimal ensemble from this pool that best fits the SAXS data. Figures 5.6.C and 5.6.D show distribution of R_g and

D_{max}, respectively, for the initial pool and the ensembles selected by EOM. In both cases, the selected structures exhibit broad distributions, indicating the contribution of compact and extended conformations to the ensemble. However, the distributions are biased towards more compact conformations relative to the random pool, suggesting the presence of attractive interactions between domains. We have confirmed that PKRΔV is flexible by fitting the SAXS data using EOM using an ensemble size of one or alternatively, by rigid body modeling of single structure using BUNCH[78]. The X^2 of the fit increases from 0.996 in the default EOM analysis to 1.303 using an ensemble of one and 1.56 using BUNCH (data not shown).

The R_g distribution and to a lesser extent, the D_{max} distribution, appears bimodal. This observation implies that PKRΔV may cluster into two families of compact and extended conformations. Consistent with this picture, the X^2 of the fit increases only slightly to 1.056 as the ensemble size is reduced to two. However, simulations indicate that such bimodal distributions may be artifactual. A continuous distribution of structures was simulated by selecting ten conformations from the pool with amplitudes derived from the pool distribution. Noise equal to the experimental PKRΔV scattering was added and the resulting simulated data set was fit using EOM with the same pool. Interestingly, the selected distribution was also bimodal and reducing the ensemble size to two results in only a marginal increase in X^2 from 1.023 to 1.040. Thus, the bimodal shape of the PKRΔV distribution does not necessarily imply the presence of two families of conformers. Repeating this process using noise-free data resulting in a selected distribution that reproduced the underlying pool more faithfully, indicating that the noise level is an important determinant of the quality of the distributions produced by EOM.

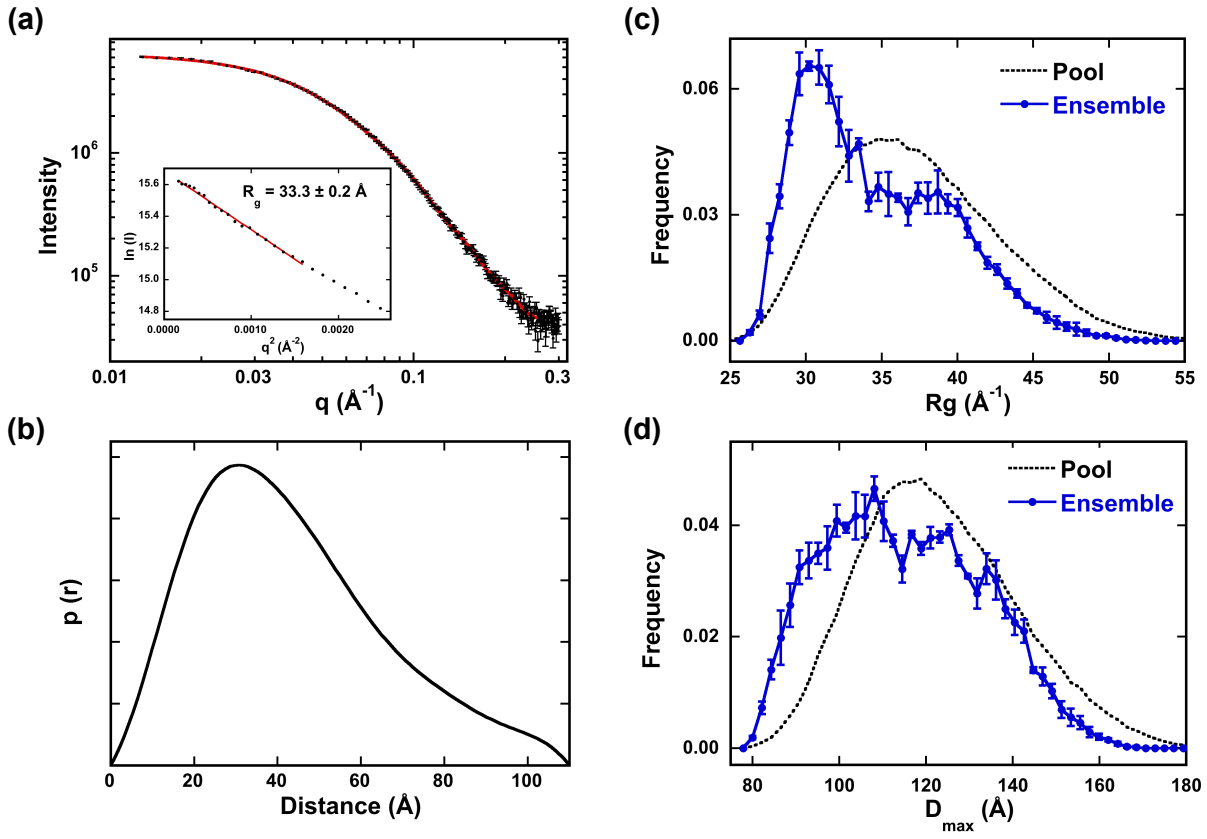

Figure 5.6. SAXS analysis of PKRΔV conformation. Data were collected at 4ºC at a protein concentration of 5 mg/ml. (a) Scattering data (points) and fit to the p(r) distribution (solid red line). Inset: Guinier analysis yields R_g = 33.3 ± 0.2 Å. (b) p(r) distance distribution produced by transforming the data in part (a) using GNOM. R_g (c) and D_{max} (d) distributions produced by fitting the the data in part (a) using EOM. The distributions of the random pool of 10,000 structures are shown in black dotted lines and the distributions selected by the genetic algorithm to fit the experimental data are shown in solid blue. The error bars correspond to the standard deviations of the distributions produced from three runs of GAJOE.

5.3. Discussion

It is noteworthy that the length of the interdomain linker in PKR orthologs is highly variable, leading to the question of how this variable region affects the structure and function of the enzyme. This region is virtually absent in *M. auratus* PKR and we initial sought to compare this construct to human PKR. However, *M. auratus* is difficult to obtain in purified form. We created an analogous deletion construct of the human enzyme, PKRΔV, which is highly homologous to the *M. auratus* enzyme and was chosen as a suitable alternative to probe the role of the variable linker. Control experiments verify that PKRΔV behaves similarly to *M. auratus* PKR.

A key observation to emerge from our analyses is that the removal of the variable region of the linker results in quantitative but not qualitative changes in the catalytic activity, RNA binding and conformational properties of PKR. The PKRΔV construct retains enzymatic activity and undergoes both RNA-independent and RNA induced phosphorylation. The enhanced autoactivation of PKRΔV indicates that the linker in human PKR negatively regulates the rate of PKR autophosphorylation. This enhancement is not simply due to higher affinity dimerization. PKR autophosphorylates at multiple sites lying within the kinase domain, the basic region and the dsRBD[58,79-81]. Potentially the variable length linker separates the domains and limits the rate with which the kinase domain catalyzes cis phosphorylation of sites within the dsRBD. Deletion of the linker may allow more rapid phosphorylation of serines and threonines in the dsRBD due to induced proximity. Alternatively, the variable region may act as a steric barrier that limits access to the sites located in the dsRBD.

As previously observed, the PKRΔV construct exhibits a bell-shape curve for activation by dsRNA where high concentrations inhibit due to dissociation of PKR dimers onto separate RNAs[12,45]. The length dependence of dsRNA activation can be correlated with binding stoichiometry: like full - length enzyme, 30 bp is the minimal length capable of binding two PKR and exhibits slight activation. The RNA binding affinities are similar to those we previously reported for PKR[59] with some enhanced affinity for the second PKR binding the 30 and 40 bp dsRNAs and detection of a third PKR binding to the 40 bp sequence. Previously, we only detected a third PKR binding to this sequence upon reducing the NaCl concentration from 200 to 75 mM. The enhanced affinities for the second and third PKR binding suggests that removal of the variable linker region enhances cooperativity of PKR assembly. The enhanced activation of PKRΔV by the 40 bp dsRNA is likely correlated with the increased binding affinity for the second and third monomers.

SAXS analysis reveals that PKRΔV retains significant conformational flexibility despite the removal of the bulk of the interdomain linker. The shapes of the Kratky plot and p(r) distribution are characteristic of proteins containing disordered regions. Structural modeling treating the regions lying between dsRBD1 and dsRBD2 and basic region as flexible linkers reveals that good fits to the scattering data require models that incorporate an ensemble of conformations. Although we cannot ascribe significance to the bimodal shapes of the R_g and D_{max} distributions, they are clearly biased towards more compact distributions that than the random pool. Similar bias was observed in our previous SAXS studies of full length PKR[34]. NMR chemical shift perturbation[18,53] measurements indicate interactions between dsRBD2 and the kinase domain that may

be responsible for the compaction of the ensemble. This interaction is weak and is expected to lead to population of both closed and open states[55]. The persistence of this conformational bias in PKRΔV implies that the basic linker region remains flexible to allow the kinase and dsRBD2 to interact; however, further investigation is require to parse the contributions of the dsRBD1-dsRBM2 linker and the basic region to the overall flexibility of the PKR.

Our observation that the structural and functional properties of PKR are not strongly affected by the presence of the variable linker region leads to the questions: why does this region exist and why do different PKR orthologs contain different length linkers? PKR is activated by a diverse array of RNAs, some of which contain extensive tertiary structure[42], and we have previously suggested that flexible tethers would permit dimerization of kinase domains and activation in cases where the dsRBDs of two PKR monomers are bound at more distal regions of the RNA activators. [34] In this case, the effects of linker length would become more pronounced for RNAs that contain duplex binding sites that are far apart. However, PKRΔV is not more susceptible than the full-length enzyme to the effects of insertion of 2'-O-Me dsRNA barriers in the middle of a 30 bp dsRNA (data not shown). Further investigation using a more diverse range of PKR ligands may reveal substantial linker dependence. Alternatively, unstructured regions are often involved in protein-protein interactions[82] and PKR is involved in a plethora of signaling pathways[9,10,83] that may be dependent on interactions with the unstructured linker.

Chapter 6: The role of the second dsRNA binding domain

6.1. Introduction

PKR contains two N-terminal dsRNA binding domains (p20) separated by a 20-residue unstructured linker. Both domains bind preferentially to A form dsRNAs[19], and the interaction is primarily non-sequence specific [18]. Although both domains comprise of a canonical αββββα motif the dsRBD1 binds dsRNA with a higher affinity than dsRBD2. However, both domains are required for the high affinity interaction (~30 fold higher) of p20 to dsRNA, thus indicating that binding is cooperative[20,84]. Most dsRBD-containing proteins possess a single copy. It is unclear if dsRBD2 plays a role exclusive of simply enhancing the overall dsRNA binding affinity. PKR is able to bind short duplexes between 16-18 bps. However, a minimum of 30 bp is required to induce PKR autophosphorylation[12,13]. NMR HSQC analyses of p20 show significant chemical shift perturbations of residues spanning both dsRBD1 and 2 upon 40 bp binding[20]. Yet, binding to 20 bp dsRNA produces perturbations within dsRBD1 and in the N terminal regions of dsRBD2. Affinity cleavage experiments performed to map the binding site for p20 and various dsRNA ligands show that both dsRBDs interact with activating dsRNAs, whereas only a single dsRBD binds to non-activating ones[51]. These results suggest that PKR activation is correlated with the binding of both dsRBDs to the dsRNA, whereas non-activating dsRNAs bind dsRBD1 and are unable to bind the entire dsRBD2. In order to elucidate the importance of the dsRBD2 we created mutations sequentially in various regions within the domain that are predicted to make dsRNA contacts. The objective of this study was to create a construct that was able to bind

dsRNA solely via the dsRBD1 regardless of the dsRNA ligand and test the importance of dsRBD2 binding on activation. dsRNA binding and activation was measured with the dsRBD2 mutants and ^{1}H-^{15}N HSQC measurements were performed to confirm that the dsRBD2 interaction was abolished.

6.2. Results

6.2.1. Rationale for the selection of dsRBD2 mutants

There is currently no structure available of the complex of PKR's dsRBD with dsRNA. A structure of a canonical Xlrbpa-2, bound to dsRNA confirmed that binding is non-sequence specific and that majority of the interactions occur between charged polar amino acids and 2'OH and phosphodiester oxygens on the dsRNA[11]. Xlrbpa-2 footprint on the dsRNA spans two minor grooves and the intervening major grove. The binding interface comprised of regions 1, 2 and 3 on Xlrbpa-2. The corresponding residues in dsRBD1 and dsRBD2 are shown in Fig. 6.1.A. Alanine substitutions in dsRBD2 were made sequentially to estimate the relative importance of each region. The locations were selected based on sequences conservation with Xlrbpa-2 and their solvent accessibility. K150A mutation was previously found to be critical for dsRNA binding[51]. A construct containing substitutions H126A, K150A and Q151A (KQH) was created to eliminate contacts predicted to occur within regions 2 and 3. A quad mutant with an additional N106A (KQHN) was made to eliminate contacts in all three regions. We chose to abolish dsRBD2 binding by making point mutations rather than deletion the domain as a whole to more closely match a physiological construct and to avoid any perturbation of PKR's overall structure or dynamics.

A)

```
                  Region 1            Region 2            Region 3
dsRBD2   101 YIGLINRIAQKKRLTVNYEQCAS-GVHGPEGFHYKCKMGQKEYSIGTGSTKQEAKQLAAKLAYLQILSE
dsRBD1    10 FMEELNTYRQKQGVVLKYQELPNSGPPHDRRFTFQVIIDGREFPEGEGRSKKEAKNAAAKLAVEILNKE
Xlrbpa2  117 --SLQELAVQKGWRLPEYTVAQESGPPHKREFTITCRVET-FVETGSGTSKQVAKRVAAEKLLTKFKT-
                 :   **     :*    . *    . *     :       * * :*: **. **:     : .
```

B)

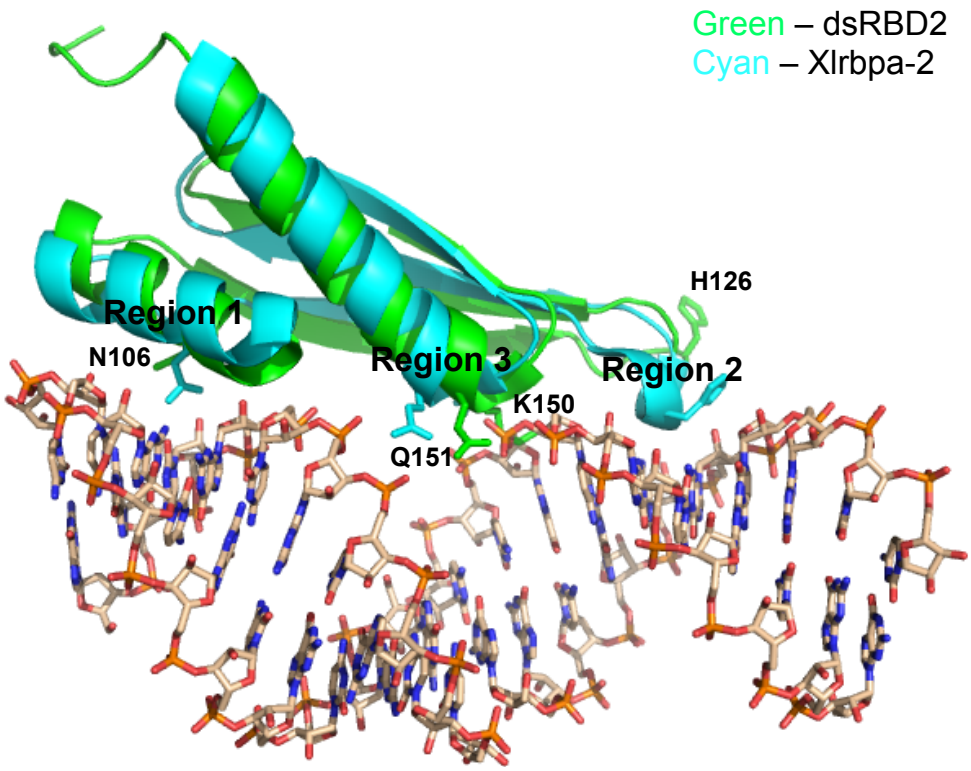

Figure 6.1. Model for intermolecular interactions between dsRBD2 and dsRNA. A) Sequence alignment of PKR dsRBD1, PKR dsRBD2 and Xlrbpa-2. Residues in regions 1 (red), 2 (blue) and 3 (green) are highlighted in bold. B) The structure of a complex of Xlrbpa-2 with dsRNA (PDB accession 1DI2) was used to develop a model for the interaction of PKR dsRBD2 with dsRNA (green). PKR dsRBD2 from the NMR structure of dsRBD1-dsRBD2 (PDB accession 1QU6) was aligned with Xlrbpa-2 and rendered in PyMol (Schrödinger). Xlrbpa-2 (ribbon, cyan), dsRNA (stick, beige), PKR dsRBD2 (ribbon, green). Key conserved residues that form the dsRNA-binding interface spanning regions 1, 2 and 3 are indicated.

6.2.2. Characterization of dsRBD2 mutants

The effects of the dsRBD2 mutations on dsRNA binding were assessed by characterizing their interaction with 40 bp dsRNA by sedimentation velocity analytical ultracentrifugation. Initally, the PKR mutants were characterized in the absence of RNA to determine homogeneity and conformation. The sedimentation coefficients of the PKR mutants were determined by fitting the sedimentation velocity data to a single species model. The sedimentation coefficients of the mutants are similar to that of WT PKR (Table XX: Show s20,w) indicating that the mutations do not perturb the native conformation of the free enzyme. All constructs bound 40 bp with a 2:1 stoichiometry, similar to WT PKR. RNA binding titrations were performed with increasing concentrations of each dsRBD2 mutant and fixed concentration of 40 bp dsRNA (0.5 μM). The K_{d1} for binding increases ~ 4 fold for the K150A mutant compared to WT PKR (Table 6.1). Mutagenesis of residues K150, Q151A and H126A, spanning regions 1 and 2 of the binding interface results in further weakening of binding (~10 fold for K_{d1}). Interestingly, K_{d2} remains unaffected. However, addition of the N106A mutation causes a ~ 4 fold decrease in K_{d2} as well. Activation of the three constructs was measured with 40 bp dsRNA (Figure 6.2). The reactions contained fixed amounts of protein (0.2 μM) and 0-3 μM of 40 bp dsRNA and they were initiated by the addition of 4 μCi of [γ-^{32}P] ATP and 0.4 mM ATP. The autoradiograms show that the KQN mutant does not exhibit an appreciable difference in dsRNA-induced autophosphorylation compared with WT PKR (Figure 6.2.A). However, the KQHN is virtually incapable of activation above background levels (Figure 6.2.B). These results indicate that either the combination of

N106A with the other mutations resulted in the complete loss of dsRBD2-dsRNA binding or that N106A alone is capable

Table 6.1. Binding constants for 40 bp and dsRBD2 mutants

PKR construct	Kd_1 (nM)	Kd_2 (nM)	RMSD[a]
K150A	162 (119, 221)	429 (350, 509)	0.0070
K150A,Q151A, H126A	484 (292, 818)	323 (241, 425)	0.0122
K150A,Q151A, H126A,N106A	341 (217, 529)	1694 (1273, 2290)	0.0106

Parameters obtained by global nonlinear least square analysis of sedimentation velocity experiments. The values in parentheses represent the 95% joint confidence intervals obtained using the F-statistic.

[a]Root mean square deviation in absorbance units

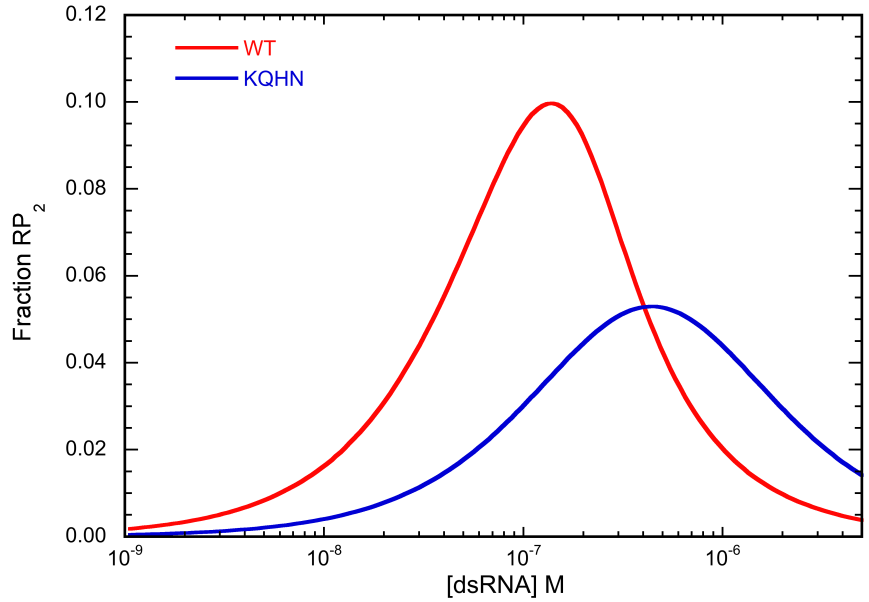

Figure 6.2: Simulation of fraction RNA-PKR_2 for wild type and KQHN PKR. The simulation was performed using IGOR Pro (Wavemetrics Inc) using the dissociation constants for WT and KQHN PKR and 40 bp dsRNA.

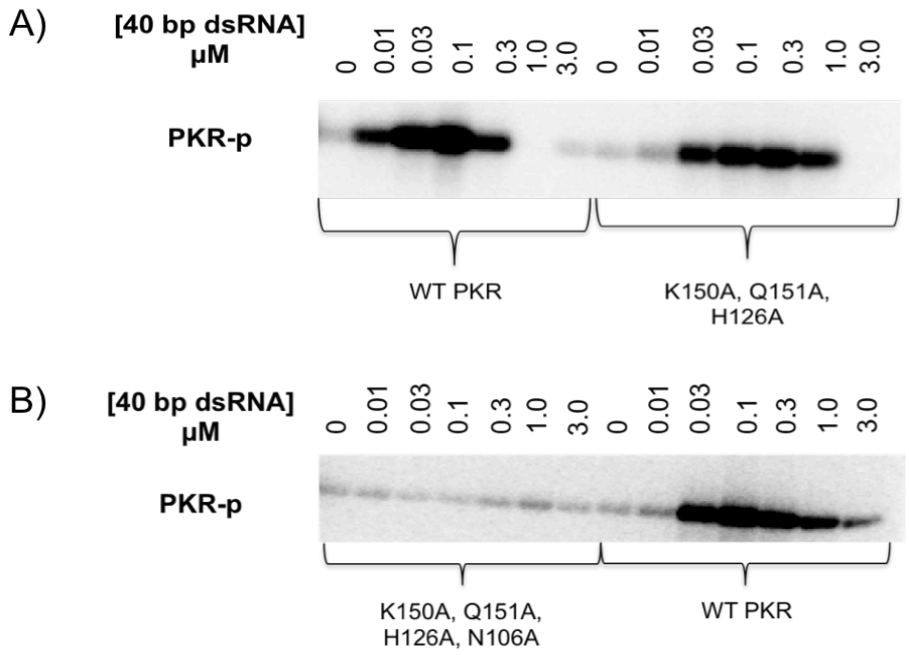

Figure 6.3: Activation of dsRBD2 mutants by 40 bp dsRNA. A) Activation of KQH PKR B) Activation of KQHN PKR. Activation assays were performed with 0.2 μM PKR and 0 – 3.0 μM 40 bp dsRNA in AU200 buffer. Reactions were initiated by adding 4 μCi of [γ-^{32}P] ATP and 0.4 mM ATP for 40 minutes at 32^{o}C. Samples were analyzed using SDS PAGE and autoradiography.

6.2.3. ^{1}H-^{15}N HSQC analysis of dsRBD

The KQHN construct was designed to abolish dsRBD2 binding to dsRNA. The decrease in binding affinity indicates that the interaction of dsRBD2 with RNA is affected, but does

not prove that binding is completely eliminated. NMR chemical shift perturbation experiments were used to directly probe PKR-RNA interactions at the single residue level. Experiments were conducted with p20 with and without KQHN subtitutions (Figure 6.4) Spectra were collected with 0.1 mM p20 and p20-KQHN under conditions used previously. The spectra were overlaid and several of the crosspeaks, mainly those in the dsRBD2 had shifted in the KQHN p20 (Figure 6.5).

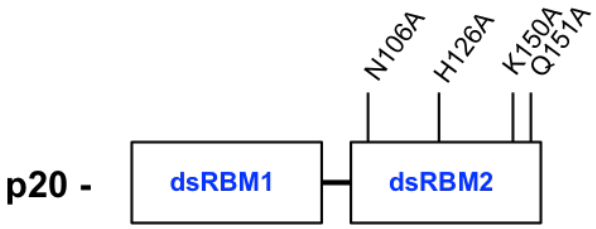

Figure 6.4: Schematic of dsRBD construct for NMR HSQC analysis. dsRBD2-dsRNA interaction or lack thereof was determined using ^{1}H-^{15}N HSQC analysis with and without 40 bp dsRNA.

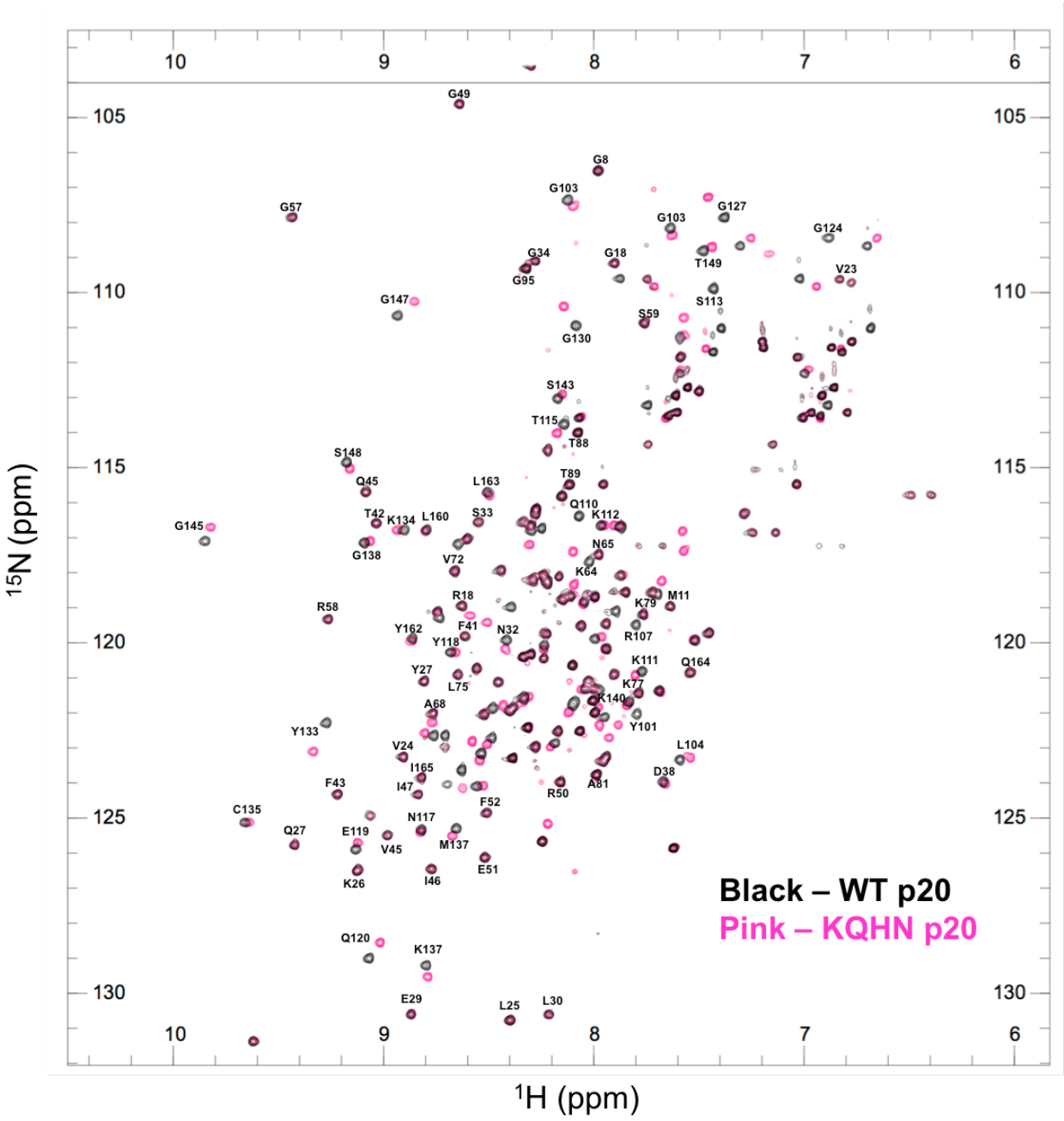

Figure 6.5: ^{1}H-^{15}N HSQC analysis of p20 and KQHN p20. The spectra were acquired on Varian Inova 800 MHz instrument with 0.1 mM p20 or quad mutation (K150A, Q151A, H126A, N106A) in 20 mM sodium phosphate, pH 6.6, 100 mM sodium chloride, 0.1 mM TCEP at 25^{o}C. Existing assignments of p20[85] were mapped onto the spectra using CcpNMR analysis [86].

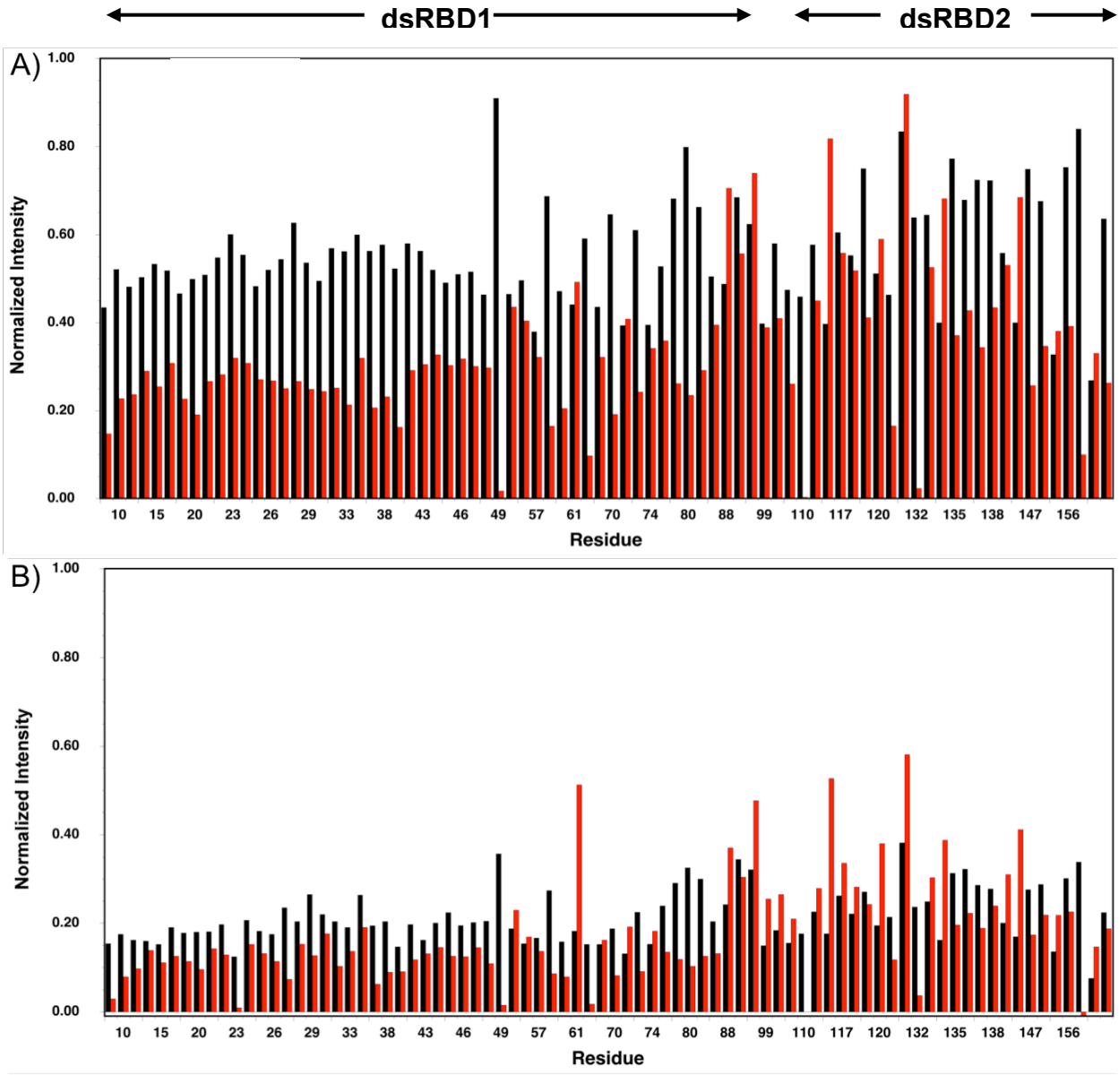

Figure 6.6: Analysis of normalized peak intensities upon dsRNA titration. Normalized intensity for p20 (black) or KQHN p20 (red) with A) 3.5 μM 40 bp dsRNA and B) 6.95 μM 40 bp dsRNA.

The spectra for p20-KQHN is well dispersed, indicating that the construct is well folded and that although the mutagenesis caused small local changes in the environment of dsRBD2 the overall conformation remained similar to WT p20. The existing ^{1}H-^{15}N HSQC spectral assignments for p20 were mapped on the spectra [18](Figure 6.5). The spectra under our conditions were slightly shifted overall compared to the original assignments, likely due to subtle changes in experimental conditions. 0.35 and 0.695 equivalents of 40 bp dsRNA was titrated into p20 and KQHN-p20 samples and the spectra were collected. No clear peak shifts were observed upon dsRNA addition, however, the overall peak intensities decreased with increasing dsRNA concentrations. The normalized intensities for the assigned residues were plotted and compared between WT p20 and KQHN p20 at each dsRNA concentration (Figure 6.6). An overall decrease of ~40% was observed with residues in dsRDB1 for WT p20 compared to ~ 80% in KQHN-p20 (Figure 6.6.A With 0.35 equivalents of 40 bp dsRNA the residues in dsRBD2 are less perturbed than dsRBD1 for both p20 and KQHN p20. However, the relative differences in perturbation in the two domains are far greater for KQHN-p20. These results may suggest that dsRBD2 in KQHN p20 may not interact directly with the dsRNA. At 0.695 equivalents of 40 bp dsRNA the intensities decreased further in dsRBD1 and dsRBD2 for both constructs. The overall reduction in the intensities may be a consequence of the formation of large heterogeneous RNA-PKR complexes in solution due to the complex equilibria for p20-RNA interaction[20]. Further HSQC analyses are required to conclusively ascertain whether dsRBD2 binds dsRNA in the KQHN construct. The overall decrease in the intensity of the cross peaks may be reduced by mixing 40 bp and p20 in stoichiometric proportions. This should produce a

homogeneous mixture of RNA-$p20_1$ species over higher order complexes such RNA-$p20_2$, RNA-$p20_3$ and RNA-$p20_4$, which are likely to contribute to the broadening of the cross peaks.

6.3. Discussion

PKR contains two tandem dsRBDs which bind variable length dsRNAs. The footprint of a single dsRBD on dsRNA is ~16 bps[18]. Only dsRNA with lengths 30 bp or higher can activate PKR. dsRBD1 binds dsRNA tighter than dsRBD2, but both motifs are required for high affinity interaction with dsRNA. NMR[20], AUC[20], and affinity cleavage[51] experiments provide evidence to suggest that dsRBD2 is required to bind to dsRNA to induce activation. To test the model we sequentially mutated key residues predicted to participate in the dsRBD2-dsRNA binding interface. Functional characterization of the mutants were performed and it was observed that KQHN did not activate with 40 bp dsRNA. The KQH mutant, however, is still active and the K_{d2} remains unaffected compared to WT PKR. The binding affinities of KQHN compared to WT PKR were weaker for K_{d1} by ~ 10 fold and ~4 fold for K_{d2}. The weakening of K_{d2} with the KQHN and not KQH may suggest that the dsRBD2 of the second PKR may bind 40 bp via region 1 alone, whereas that of the first PKR binds via all three regions. The abolishing of activation with the KQHN mutant may be due to a cumulative effect of mutating all three regions of the dsRBD2. Alternately, the effect could be due to N106A alone, suggesting that it is a key regulatory residue in the dsRNA binding and activation. Further characterization of a single N106A mutant is required to ascertain the role of N106 in PKR activation. Viral and cellular RNAs with complex secondary structures are able to bind and activate PKR. dsRNAs containing 2'-O-methyl barriers between 15 bp

duplex stretches are able to bind two PKRs but do not induce activation(Bushra Husain, Stephen Hesler, James Cole; 2015). Notably, differences in the dsRNA structure and composition can translate to inability for PKR activation suggesting a mechanism for inter-domain communication. This may occur either through the inter-domain linker or perhaps through transient interactions between dsRBD2 and the kinase domain. In such as scenario, the role of the dsRBD2 may be more significant than to simply serve as a redundant domain required for high affinity binding of the dsRBD to dsRNA through cooperative assembly.

Chapter 6: Conclusions and future direction

During viral infection PKR recognizes RNAs that possess an array of complex secondary structural elements such as bulges, loops and mismatches[68]. Despite PKRs preference for duplex stretches of dsRNA it is still able to bind and become activated by structured RNAs. Viruses synthesize decoy RNAs such as VAI from Adenovirus and EBER1 and EBER2 from Epstein Barr virus, which bind and sequester PKRs in solution minimizing the PKR-mediated response[87,88]. An elusive aspect of this inhibition process is the ability for PKR to distinguish non-activating and activating RNAs, since many of them possess similar structural features.

The assembly of more than one PKR on a dsRNA is critical since activation is linked closely with dimerization. A FRET–based dimerization assay was presented (Chapter 4) which allowed us to directly probe PKR dimerization upon dsRNA binding. The results showed that dsRNAs containing fairly short stretches of 2'O-methyl RNA between 15 bp duplex regions are able to bind two PKRs, but don't activate. Interestingly, these RNAs induced dimerization. Dimer interface mutants R262D and Y323A were previously thought to be catalytically inactive due to their inability to dimerize[17]. However, we observed that both mutants dimerize upon dsRNA binding as well as in the absence of dsRNA. Our results reveal the presence of a novel inactive dimer species that may serve to regulate its activation when bound to a specific dsRNA ligand. Interestingly, the dsRNA structure can affect the nature of the dimer configuration. A specific back-to-back dimer is critical for PKR activation.

PKR belongs to a family of eIF2α kinases. PERK[60] (PKR-like endoplasmic reticulum kinase) and PKR exist as unphosphorylated monomers in solution. In the presence of an activating dsRNA they form the back-to-back dimer and become active. GCN2 [62](general control non-derepressible 2) and HRI[61] (heme-regulated inhibitor kinase) exist as constitutive inactive dimers in solution. However, a rearrangement of their dimer interface is required for activation. Since the eIF2α kinases participate in a myriad of pathways that eventually lead to cell death, activation must be tightly regulated within the cell. Inactive dimer configurations may exist to lock the kinases and prevent any aberrant or background activation. High throughput transcriptional analysis show that human cells can produce hundred of dsRNA[74]. PKR-dsRNA binding is non-sequence specific and under low salt conditions even short RNAs can bind more than one PKR[13,59]. Inactive PKR dimers may form to prevent inappropriate activation upon binding to host dsRNA ligands. The nature of the inactive dimer interface, however, remains elusive. Dimerization assays performed using a FRET pair at position 301 instead of 261 demonstrate that PKR does not form a GCN2-like antiparallel inactive dimer interface. Future experiments to probe the inactive dimer interface can involve the characterization of PKR constructs with FRET pairs at several different locations on the kinase dimer. Alternately, high resolution structural analyses of catalytically inactive mutants R262D or Y323A mutants will likely answer the questions pertaining to the specific inactive dimer interface.

Although PKR activation has been studied extensively, the precise mechanism of autophosphorylation is elusive since the active dimer is oriented such that the active site clefts are facing away from each other. *Cis*-phosphorylation of T446 has been

suggested as a likely first step in activation followed by the trans-autophosphorylation at multiple serine and threonine sites making the enzyme fully active[65]. To test the various binding interfaces of the kinase domains at different stages in activation a number of FRET pair containing constructs can be designed and assayed. For example, FRET pairs can be incorporated that show enhanced energy transfer when a front-to-back or front-to-front interface is formed.

The isolation and high-resolution characterization of dimeric PKR species is challenging since they are interact weakly and reversibly in solution. The creation of constructs with strategically placed cysteine pairs can allow us to trap dimers via disulfide bonding, and purify them for biophysical or structural characterization.

PKR contains a ~90 residues interdomain linker. The N-terminal regions (169-228) is variable in length across different orthologs and is absent in hamster PKR. The C-terminal end is shorter and is enriched in positively charged residues. AFM[56], NMR[35] and SAXS[34] analysis show that PKR exists in ensemble of conformations likely due to the disorder in the linker. The linker also presents a challenge for the crystallization of the full-length enzyme. To define the role of the linker we created linker-deleted constructs PKRΔV and PKRΔVB and functionally characterized them (Chapter 5). PKRΔV autophosphoryalates in the absence of dsRNA much more potently than WT PKR. In addition, it binds to 40 bp dsRNA with a higher stoichiometry than WT PKR. Overall, the construct is potently active since increased dsRNA binding stoichiometries are directly correlation with higher levels of activation. These results suggest that the long unstructured linker serves to negatively regulate PKR activation by curbing background autophosphorylation and limiting PKR assembly on dsRNAs. L18 protein of

the 60 S ribosomal unit, which is overexpressed in patients with colorectal cancer sequesters PKR via the dsRNA binding domain and prevents it from activating[89]. This indicates that the cells likely employ several pathways to negatively regulate PKR activity.

The linker-deleted constructs of PKR have thus far only been characterized with duplex RNAs. They may play a role in recognizing secondary structural elements of RNAs that exist and bind PKR *in vivo.* Further experiments can be conducted to characterize the role of the linker in recognition of structured RNAs or ss-dsRNAs. One of the most well studied consequences of PKR activation is eIF2α phosphorylation. However, PKR participates in several pathways involving cell differentiation, cell growth, heat shock stress, UV stress, bacterial infection, etc. It is possible that the linker may play a larger role in signaling and other downstream processes.

Most dsRBD-containing proteins possess a single copy. The footprint of a dsRBD on a dsRNA is 16 bps. Yet, PKR, which has two such dsRBDs is able to bind 20 bp dsRNAs in a 2:1 stoichiometry. Interestingly, these dsRNAs do not induce activation. NMR[20] and AUC analyses demonstrate that the inability to activate is due to the impaired dsRBD2 binding. We tested this model by mutating residues within the dsRBD2 that are predicted to bind dsRNA based on sequence and structural homology with Xlrbpa2 (Chapter 6). The quad mutant K150A, Q151A, H126A, N106A is able to bind PKR in a 2:1 stoichiometry but does not activate. These results suggest that specific contacts made between the dsRBD2 and dsRNA are essential for dsRNA-induced PKR activation. Interestingly, the triple mutant K150A, Q151A, H126A is able to activate suggesting that N106A may play a key role in dsRNA-induced activation.

Ongoing experiments in the lab involve the functional characterization of N106A single mutant. More detailed chemical shift measurements also need to be performed with p20 WT and quad mutant constructs to ascertain if the mutations are blocking dsRBD2 binding.

In summation, we have developed a reproducible and reliable FRET-based assay to measure dimerization of PKR upon dsRNA binding. This assay with can be used with virtually any ligand as long as the anisotropy differences elicited by depolarization are large enough and measurable. Our assays reveal a novel inactive dimer species, which may exist as a mechanism for PKR to distinguish host and viral dsRNAs. We have determined that the unstructured linker serves to negatively regulate PKR activation in the absence of an appropriate stimulus. The role of the second dsRBD has also been explored. Mutation of residues predicted to lie within the dsRBD-dsRNA interface block PKR activation, but reduce dsRNA binding affinity by ~4 fold compared to WT PKR. These results suggest that a dsRBD2 mediated dsRNA binding may be key for activation, and that PKR may distinguish activating and non-activating dsRNAs based on the relative affinity of the dsRBD2.

References

(1) Stark, G. R., Kerr, I. M., Williams, B. R., Silverman, R. H., and Schreiber, R. D. (1998) How cells respond to interferons. *Annu Rev Biochem 67*, 227–264.

(2) Ben-Asouli, Y., Banai, Y., Pel-Or, Y., Shir, A., and Kaempfer, R. (2002) Human interferon-gamma mRNA autoregulates its translation through a pseudoknot that activates the interferon-inducible protein kinase PKR. *Cell 108*, 221–232.

(3) Toth, A. M., Zhang, P., Das, S., George, C. X., and Samuel, C. E. (2006) Interferon action and the double-stranded RNA-dependent enzymes ADAR1 adenosine deaminase and PKR protein kinase. *Prog. Nucleic Acid Res. Mol. Biol. 81*, 369–434.

(4) Bowie, A. G., and Unterholzner, L. (2008) Viral evasion and subversion of pattern-recognition receptor signalling. *Nat Rev Immunol 8*, 911–922.

(5) Robertson, H. D., and Mathews, M. B. (1996) The regulation of the protein kinase PKR by RNA. *Biochimie 78*, 909–914.

(6) Taylor, S. S., Haste, N. M., and Ghosh, G. (2005) PKR and eIF2alpha: integration of kinase dimerization, activation, and substrate docking. *Cell 122*, 823–825.

(7) Proud, C. G. (1995) PKR: a new name and new roles. *Trends Biochem Sci 20*, 241–246.

(8) Williams, B. R. G. (1999) PKR; a sentinal kinase for cellular stress. *Oncogene 18*, 6112–6120.

(9) García, M. A., Gil, J., Ventoso, I., Guerra, S., Domingo, E., Rivas, C., and Esteban, M. (2006) Impact of protein kinase PKR in cell biology: from antiviral to antiproliferative action. *Microbiology and Molecular Biology Reviews 70*, 1032–1060.

(10) Pindel, A. (2010) The role of protein kinase R in the interferon response. *Journal of*

Interferon & Cytokine Research.

(11) Ryter, J. M., and Schultz, S. C. (1998) Molecular basis of double-stranded RNA-protein interactions: structure of a dsRNA-binding domain complexed with dsRNA. *EMBO J 17*, 7505–7513.

(12) Manche, L., Green, S. R., Schmedt, C., and Mathews, M. B. (1992) Interactions between double-stranded RNA regulators and the protein kinase DAI. *Mol Cell Biol 12*, 5238–5248.

(13) Lemaire, P. A., Anderson, E., Lary, J., and Cole, J. L. (2008) Mechanism of PKR Activation by dsRNA. *J Mol Biol 381*, 351–360.

(14) O'Malley, R. P., Mariano, T. M., Siekierka, J., and Mathews, M. B. (1986) A mechanism for the control of protein synthesis by adenovirus VA RNAI. *Cell 44*, 391–400.

(15) Hunter, T., Hunt, T., Jackson, R. J., and Robertson, H. D. (1975) The characteristics of inhibition of protein synthesis by double-stranded ribonucleic acid in reticulocyte lysates. *J Biol Chem 250*, 409–417.

(16) Weber, F., Wagner, V., Rasmussen, S. B., Hartmann, R., and Paludan, S. R. (2006) Double-stranded RNA is produced by positive-strand RNA viruses and DNA viruses but not in detectable amounts by negative-strand RNA viruses. *Journal of Virology 80*, 5059–5064.

(17) Dar, A., Dever, T., and Sicheri, F. (2005) Higher-Order Substrate Recognition of eIF2α by the RNA-Dependent Protein Kinase PKR. *Cell 122*, 887–900.

(18) Nanduri, S., Carpick, B. W., Yang, Y., Williams, B. R., and Qin, J. (1998) Structure of the double-stranded RNA binding domain of the protein kinase PKR reveals the

molecular basis of its dsRNA-mediated activation. *EMBO J 17*, 5458–5465.

(19) Bevilacqua, P. C., and Cech, T. R. (1996) Minor-groove recognition of double-stranded RNA by the double-stranded RNA-binding domain from the RNA-activated protein kinase PKR. *Biochemistry 35*, 9983–9994.

(20) Ucci, J. W., Kobayashi, Y., Choi, G., Alexandrescu, A. T., and Cole, J. L. (2007) Mechanism of interaction of the double-stranded RNA (dsRNA) binding domain of protein kinase R with short dsRNA sequences. *Biochemistry 46*, 55–65.

(21) Toroney, R., Nallagatla, S. R., Boyer, J. A., Cameron, C. E., and Bevilacqua, P. C. (2010) Regulation of PKR by HCV IRES RNA: importance of domain II and NS5A. *J Mol Biol 400*, 393–412.

(22) Shimoike, T., McKenna, S. A., Lindhout, D. A., and Puglisi, J. D. (2009) Translational insensitivity to potent activation of PKR by HCV IRES RNA. *Antiviral Res 83*, 228–237.

(23) Osman, F., Jarrous, N., Ben-Asouli, Y., and Kaempfer, R. (1999) A cis-acting element in the 3'-untranslated region of human TNF-alpha mRNA renders splicing dependent on the activation of protein kinase PKR. *Genes Dev 13*, 3280–3293.

(24) Vuyisich, M., Spanggord, R. J., and Beal, P. A. (2002) The binding site of the RNA-dependent protein kinase (PKR) on EBER1 RNA from Epstein-Barr virus. *EMBO Rep 3*, 622–627.

(25) Mellits, K. H., Kostura, M., and Mathews, M. B. (1990) Interaction of adenovirus VA RNAI with the protein kinase DAI: nonequivalence of binding and function. *Cell 61*, 843–852.

(26) Furtado, M. R., Subramanian, S., Bhat, R. A., Fowlkes, D. M., Safer, B., and

Thimmappaya, B. (1989) Functional dissection of adenovirus VAI RNA. *Journal of Virology 63*, 3423–3434.

(27) Rahman, A., Malhotra, P., Dhar, R., Kewalramani, T., and Thimmapaya, B. (1995) Effect of single-base substitutions in the central domain of virus-associated RNA I on its function. *Journal of Virology 69*, 4299–4307.

(28) Carpick, B. W., Graziano, V., Schneider, D., Maitra, R. K., Lee, X., and Williams, B. R. (1997) Characterization of the solution complex between the interferon-induced, double-stranded RNA-activated protein kinase and HIV-I trans-activating region RNA. *J Biol Chem 272*, 9510–9516.

(29) Maitra, R. K., McMillan, N. A., Desai, S., McSwiggen, J., Hovanessian, A. G., Sen, G., Williams, B. R., and Silverman, R. H. (1994) HIV-1 TAR RNA has an intrinsic ability to activate interferon-inducible enzymes. *Virology 204*, 823–827.

(30) Heinicke, L. A., Wong, C. J., Lary, J., Nallagatla, S. R., Diegelman-Parente, A., Zheng, X., Cole, J. L., and Bevilacqua, P. C. (2009) RNA dimerization promotes PKR dimerization and activation. *J Mol Biol 390*, 319–338.

(31) Lemaire, P. A., Lary, J., and Cole, J. L. (2005) Mechanism of PKR activation: dimerization and kinase activation in the absence of double-stranded RNA. *J Mol Biol 345*, 81–90.

(32) Romano, P. R., Garcia-Barrio, M. T., Zhang, X., Wang, Q., Taylor, D. R., Zhang, F., Herring, C., Mathews, M. B., Qin, J., and Hinnebusch, A. G. (1998) Autophosphorylation in the activation loop is required for full kinase activity in vivo of human and yeast eukaryotic initiation factor 2a kinases PKR and GCN2. *Mol Cell Biol 18*, 2282–2297.

(33) Taylor, D. R., Lee, S. B., Romano, P. R., Marshak, D. R., Hinnebusch, A. G.,

Esteban, M., and Mathews, M. B. (1996) Autophosphorylation sites participate in the activation of the double-stranded-RNA-activated protein kinase PKR. *Mol Cell Biol 16*, 6295–6302.

(34) Vanoudenhove, J., Anderson, E., Krueger, S., and Cole, J. L. (2009) Analysis of PKR structure by small-angle scattering. *J Mol Biol 387*, 910–920.

(35) McKenna, S. A., Lindhout, D. A., Kim, I., Liu, C. W., Gelev, V. M., Wagner, G., and Puglisi, J. D. (2007) Molecular framework for the activation of RNA-dependent protein kinase. *J Biol Chem 282*, 11474–11486.

(36) Wong, C. J., Launer-Felty, K., and Cole, J. L. (2011) Analysis of PKR-RNA interactions by sedimentation velocity. *Meth Enzymol 488*, 59–79.

(37) Cole, J. L., Lary, J. W., P Moody, T., and Laue, T. M. (2008) Analytical ultracentrifugation: sedimentation velocity and sedimentation equilibrium. *Methods in Cell Biology 84*, 143–179.

(38) Runnels, L. W., and Scarlata, S. F. (1995) Theory and application of fluorescence homotransfer to melittin oligomerization. *Biophys J 69*, 1569–1583.

(39) Szabó, A., Horvath, G., Szöllosi, J., and Nagy, P. (2008) Quantitative characterization of the large-scale association of ErbB1 and ErbB2 by flow cytometric homo-FRET measurements. *Biophys J 95*, 2086–2096.

(40) Langland, J. O., Cameron, J. M., Heck, M. C., Jancovich, J. K., and Jacobs, B. L. (2006) Inhibition of PKR by RNA and DNA viruses. *Virus Research 119*, 100–110.

(41) Tian, B., Bevilacqua, P. C., Diegelman-Parente, A., and Mathews, M. B. (2004) The double-stranded-RNA-binding motif: interference and much more. *Nat Rev Mol Cell Biol 5*, 1013–1023.

(42) Nallagatla, S. R., Toroney, R., and Bevilacqua, P. C. (2011) Regulation of innate immunity through RNA structure and the protein kinase PKR. *Curr Opin Struct Biol 21*, 119–127.

(43) Cole, J. L. (2007) Activation of PKR: an open and shut case? *Trends Biochem Sci 32*, 57–62.

(44) Dey, M., Cao, C., Dar, A. C., Tamura, T., Ozato, K., Sicheri, F., and Dever, T. E. (2005) Mechanistic link between PKR dimerization, autophosphorylation, and eIF2alpha substrate recognition. *Cell 122*, 901–913.

(45) Kostura, M., and Mathews, M. B. (1989) Purification and activation of the double-stranded RNA-dependent eIF-2 kinase DAI. *Mol Cell Biol 9*, 1576–1586.

(46) Ucci, J. W., and Cole, J. L. (2004) Global analysis of non-specific protein-nucleic interactions by sedimentation equilibrium. *Biophys Chem 108*, 127–140.

(47) Cole, J. L. (2004) Analysis of heterogeneous interactions. *Meth Enzymol 384*, 212–232.

(48) Epstein, I. R. (1978) Cooperative and non-cooperative binding of large ligands to a finite one-dimensional lattice: a model for ligand-oligonucleotide interactions. *Biophys Chem 8*, 327–339.

(49) Latt, S. A., and Sober, H. A. (1967) Protein-nucleic acid interactions. II. Oligopeptide-polyribonucleotide binding studies. *Biochemistry 6*, 3293–3306.

(50) Munro, P. D., Jackson, C. M., and Winzor, D. J. (2000) Consequences of the non-specific binding of a protein to a linear polymer: reconciliation of stoichiometric and equilibrium titration data for the thrombin-heparin interaction. *J .Theor. Biol. 203*, 407–418.

(51) Spanggord, R. J., Vuyisich, M., and Beal, P. A. (2002) Identification of binding sites for both dsRBMs of PKR on kinase-activating and kinase-inhibiting RNA ligands. *Biochemistry 41*, 4511–4520.

(52) Masliah, G., Barraud, P., and Allain, F. H.-T. (2013) RNA recognition by double-stranded RNA binding domains: a matter of shape and sequence. *Cell. Mol. Life Sci. 70*, 1875–1895.

(53) Gelev, V., Aktas, H., Marintchev, A., Ito, T., Frueh, D., Hemond, M., Rovnyak, D., Debus, M., Hyberts, S., Usheva, A., Halperin, J., and Wagner, G. (2006) Mapping of the auto-inhibitory interactions of protein kinase R by nuclear magnetic resonance. *J. Mol. Biol. 364*, 352–363.

(54) Nanduri, S., Rahman, F., Williams, B. R., and Qin, J. (2000) A dynamically tuned double-stranded RNA binding mechanism for the activation of antiviral kinase PKR. *EMBO J 19*, 5567–5574.

(55) Anderson, E., and Cole, J. L. (2008) Domain stabilities in protein kinase R (PKR): evidence for weak interdomain interactions. *Biochemistry 47*, 4887–4897.

(56) Lemaire, P. A., Tessmer, I., Craig, R., Erie, D. A., and Cole, J. L. (2006) Unactivated PKR exists in an open conformation capable of binding nucleotides. *Biochemistry 45*, 9074–9084.

(57) Lavoie, H., Li, J. J., Thevakumaran, N., Therrien, M., and Sicheri, F. (2014) Dimerization-induced allostery in protein kinase regulation. *Trends Biochem Sci 39*, 475–486.

(58) Zhang, F., Romano, P. R., Nagamura-Inoue, T., Tian, B., Dever, T. E., Mathews, M. B., Ozato, K., and Hinnebusch, A. G. (2001) Binding of double-stranded RNA to

protein kinase PKR is required for dimerization and promotes critical autophosphorylation events in the activation loop. *J Biol Chem 276*, 24946–24958.

(59) Husain, B., Mukerji, I., and Cole, J. L. (2012) Analysis of high-affinity binding of protein kinase R to double-stranded RNA. *Biochemistry 51*, 8764–8770.

(60) Bertolotti, A., Zhang, Y., Hendershot, L. M., Harding, H. P., and Ron, D. (2000) Dynamic interaction of BiP and ER stress transducers in the unfolded-protein response. *Nat Cell Biol 2*, 326–332.

(61) Yang, J. M., London, I. M., and Chen, J. J. (1992) Effects of hemin and porphyrin compounds on intersubunit disulfide formation of heme-regulated eIF-2 alpha kinase and the regulation of protein synthesis in reticulocyte lysates. *J Biol Chem 267*, 20519–20524.

(62) Qiu, H., Garcia-Barrio, M. T., and Hinnebusch, A. G. (1998) Dimerization by translation initiation factor 2 kinase GCN2 is mediated by interactions in the C-terminal ribosome-binding region and the protein kinase domain. *Mol Cell Biol 18*, 2697–2711.

(63) Cui, W., Li, J., Ron, D., and Sha, B. (2011) The structure of the PERK kinase domain suggests the mechanism for its activation. *Acta Crystallogr D Biol Crystallogr 67*, 423–428.

(64) Padyana, A. K., Qiu, H., Roll-Mecak, A., Hinnebusch, A. G., and Burley, S. K. (2005) Structural basis for autoinhibition and mutational activation of eukaryotic initiation factor 2alpha protein kinase GCN2. *J Biol Chem 280*, 29289–29299.

(65) Dey, M., Mann, B. R., Anshu, A., and Mannan, M. A.-U. (2014) Activation of Protein Kinase PKR Requires Dimerization-induced cis-Phosphorylation within the Activation Loop. *Journal of Biological Chemistry 289*, 5747–5757.

(66) Dey, M., Cao, C., Sicheri, F., and Dever, T. E. (2007) Conserved intermolecular salt bridge required for activation of protein kinases PKR, GCN2, and PERK. *J Biol Chem 282*, 6653–6660.

(67) Young, T. S., Ahmad, I., Yin, J. A., and Schultz, P. G. (2010) An enhanced system for unnatural amino acid mutagenesis in E. coli. *J Mol Biol 395*, 361–374.

(68) Heinicke, L. A., Nallagatla, S. R., Hull, C. M., and Bevilacqua, P. C. (2011) RNA helical imperfections regulate activation of the protein kinase PKR: effects of bulge position, size, and geometry. *RNA 17*, 957–966.

(69) Patel, S., Blose, J. M., Sokoloski, J. E., Pollack, L., and Bevilacqua, P. C. (2012) Specificity of the double-stranded RNA-binding domain from the RNA-activated protein kinase PKR for double-stranded RNA: insights from thermodynamics and small-angle X-ray scattering. *Biochemistry 51*, 9312–9322.

(70) Heinicke, L. A., and Bevilacqua, P. C. (2012) Activation of PKR by RNA misfolding: HDV ribozyme dimers activate PKR. *RNA 18*, 2157–2165.

(71) Minks, M. A., West, D. K., Benvin, S., Greene, J. J., Ts'o, P. O. P., and Baglioni, C. (1980) Activation of 2'-5‘-oligo-(A) polymerase and protein kinase of interferon-treated HeLa cells by 2’-O-methylated poly(inosinic acid)-poly(cytidylic acid). *J Biol Chem 255*, 6403–6407.

(72) Koh, H. R., Kidwell, M. A., Ragunathan, K., Doudna, J. A., and Myong, S. (2013) ATP-independent diffusion of double-stranded RNA binding proteins. *Proc Natl Acad Sci USA 110*, 151–156.

(73) Li, F. Z., Li, S. W., Wang, Z., Shen, Y. Q., Zhang, T. C., and Yang, X. (2013) Structure of the kinase domain of human RNA-dependent protein kinase with K296R

mutation reveals a face-to-face dimer. *Chinese Science Bulletin 58*, 998–1002.

(74) Portal, M. M., Pavet, V., Erb, C., and Gronemeyer, H. (2015) Human cells contain natural double-stranded RNAs with potential regulatory functions. *Nat Struct Mol Biol 22*, 89–97.

(75) Gouy, M., Guindon, S., and Gascuel, O. (2010) SeaView version 4: A multiplatform graphical user interface for sequence alignment and phylogenetic tree building. *Mol. Biol. Evol. 27*, 221–224.

(76) Tria, G., Mertens, H. D. T., Kachala, M., and Svergun, D. I. (2015) Advanced ensemble modelling of flexible macromolecules using X-ray solution scattering. *IUCrJ 2*, 207–217.

(77) Bernadó, P., Mylonas, E., Petoukhov, M. V., Blackledge, M., and Svergun, D. I. (2007) Structural characterization of flexible proteins using small-angle X-ray scattering. *J Am Chem Soc 129*, 5656–5664.

(78) Petoukhov, M. V., and Svergun, D. I. (2005) Global rigid body modeling of macromolecular complexes against small-angle scattering data. *Biophys J 89*, 1237–1250.

(79) Zhang, X., Herring, C. J., Romano, P. R., Szczepanowska, J., Brzeska, H., Hinnebusch, A. G., and Qin, J. (1998) Identification of phosphorylation sites in proteins separated by polyacrylamide gel electrophoresis. *Anal Chem 70*, 2050–2059.

(80) Taylor, D. R., Tian, B., Romano, P. R., Hinnebusch, A. G., Lai, M. M., and Mathews, M. B. (2001) Hepatitis C virus envelope protein E2 does not inhibit PKR by simple competition with autophosphorylation sites in the RNA-binding domain. *Journal of Virology 75*, 1265–1273.

(81) Romano, P. R., Garcia-Barrio, M. T., Zhang, X., Wang, Q., Taylor, D. R., Zhang, F., Herring, C., Mathews, M. B., Qin, J., and Hinnebusch, A. G. (1998) Autophosphorylation in the activation loop is required for full kinase activity in vivo of human and yeast eukaryotic initiation factor 2alpha kinases PKR and GCN2. *Mol Cell Biol 18*, 2282–2297.

(82) Oldfield, C. J., and Dunker, A. K. (2014) Intrinsically disordered proteins and intrinsically disordered protein regions. *Annu Rev Biochem 83*, 553–584.

(83) Lu, B., Nakamura, T., Inouye, K., Li, J., Tang, Y., Lundbäck, P., Valdes-Ferrer, S. I., Olofsson, P. S., Kalb, T., Roth, J., Zou, Y., Erlandsson-Harris, H., Yang, H., Ting, J. P. Y., Wang, H., Andersson, U., Antoine, D. J., Chavan, S. S., Hotamisligil, G. S., and Tracey, K. J. (2012) Novel role of PKR in inflammasome activation and HMGB1 release. *Nature 488*, 670–674.

(84) Tian, B., and Mathews, M. B. (2001) Functional characterization of and cooperation between the double-stranded RNA-binding motifs of the protein kinase PKR. *J Biol Chem 276*, 9936–9944.

(85) Nanduri, S., Carpick, B., Yang, Y., Williams, B. R. G., and Qin, J. (1998) 1H, 13C, 15N resonance assignments of the 20 kDa double stranded RNA binding domain of PKR. *J Biomol NMR 12*, 349–351.

(86) Vranken, W. F., Boucher, W., Stevens, T. J., Fogh, R. H., Pajon, A., Llinas, M., Ulrich, E. L., Markley, J. L., Ionides, J., and Laue, E. D. (2005) The CCPN data model for NMR spectroscopy: development of a software pipeline. *Proteins 59*, 687–696.

(87) Kitajewski, J., Schneider, R. J., Safer, B., Munemitsu, S. M., Samuel, C. E., Thimmappaya, B., and Shenk, T. (1986) Adenovirus VAI RNA antagonizes the antiviral action of interferon by preventing activation of the interferon-induced eIF-2 alpha kinase.

Cell 45, 195–200.

(88) Clemens, M. J., Liang, K. G., Jeffrey, I. W., Schofield, A., Sharp, T. V., Elia, A., Matys, V., James, M. C., and Tilleray, V. J. (1994) Regulation of the interferon-inducible eIF-2a protein kinase by small RNAs. *Biochimie 76*, 770–778.

(89) Kumar, K. U., Srivastava, S. P., and Kaufman, R. J. (1999) Double-stranded RNA-activated protein kinase (PKR) is negatively regulated by 60S ribosomal subunit protein L18. *Mol Cell Biol 19*, 1116–1125.